in ES-ACM, some cells showed tyrosine hydroxylase (TH) - immunoreactivity (Figure 4B). Furthermore, when cultured in ES-ACM again, the cells could differentiate into astrocytes via formation of spheres. To induce differentiation of neural stem cells into astrocytes, the culture medium was changed from NSCM to G5 medium. After medium change, most neural stem cells had the appearance of typical astrocytes. By 2 weeks culture in G5 medium, the majority (82.4±1.8%, $n = 3$) of cells expressed GFAP, and few (<1%) expressed MAP2.

Electrophysiological analysis of neurons differentiated from hES cells

For electrophysiological study, hES-derived neurons were cultured on coverslips for 4–6 weeks. The coverslips were transferred to a recording chamber before use. Neurons were selected based on their appearance (spherical shape with long neurites). The resting membrane potential of the neurons were −62.0~−11.1 mV ($n = 26$). Among 26 cells examined, action potentials were elicited in 22 cells (Figure 5A, Control). Application of 1 μM tetrodotoxin (TTX) completely suppressed the overshoot (Figure 5A, right panel). The action potentials were evoked only when resting membrane potentials were set to −70 mV by current injection in 11 cells. The rest of the cells did not possess membrane excitability ($n = 4$ out of 26, closed circle in Figure 5B).

Survival of hES cell-derived neurons in mice brain

To examine differentiation of hES cell-derived cells *in vivo*, we transplanted neural stem cells induced with ES-ACM into mice brain ($n = 7$). Before transplantation, the majority (85.1±5.1%, $n = 4$) of donor cells expressed Nestin, a marker for neural stem cell (Figure 6A), and no cells expressed octamer transcription factor-3 (Oct-3) and stage-specific embryonic antigen (SSEA-4), two makers for undifferentiated cells (data not shown). Four weeks after engraftment, many ($2–3 \times 10^2$) hrGFP-positive cells were recognized (Figure 6B, C). Some of these cells (<10%) were also Tuj1-immunoreactive (Figure 6D). In the vicinity of the grafts, few cells were immunoreactive against Ki-67, a marker for proliferation. However, none of these Ki-67-positive cells were positive for hrGFP (Figure 6E). Teratoma was not detected in any of the transplanted mice.

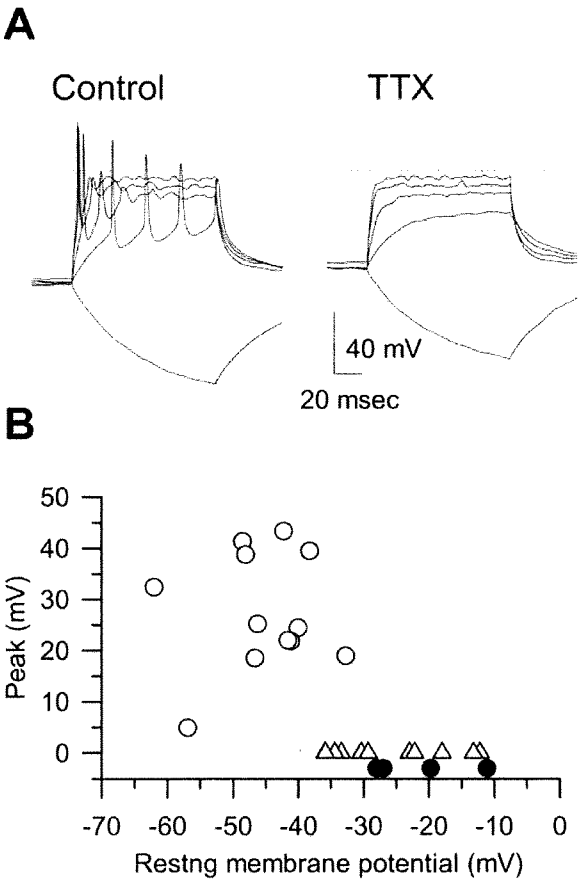

Figure 5. Electrophysiological properties of hES-derived neurons. (A): (Control) Action potentials elicited by depolarizing current injections (50 pA steps for 100 msec). The resting membrane potential was −62.0 mV. During the hyperpolarizing pulse (−50 pA), no 'sug' component was observed. (TTX) Membrane potentials recorded in the presence of 1 μM tetrodotoxin. In both panels, the dotted lines indicate 0 mV. (B): Summary of the resting membrane potentials and the peak amplitudes. Open circle; cells with action potentials. Open triangle; cells with action potentials only when the resting membrane potential was set to −70 mV. Closed circle; cells without membrane excitability.
doi:10.1371/journal.pone.0006318.g005

Discussion

We have shown in this study that neurons and astrocytes can be produced efficiently from hES cells using a conditioned medium collected from either rat primary-cultured astrocytes or hES cell-derived astrocytes. Astrocytes derived from hES cells can be used for continuous generation of neurons. Although a number of media including serum-free media supplemented with various cytokines and/or growth factors have been developed [10,11] to keep a long-term culture of neuronal cells, synthetic culture systems can usually maintain neural cells stable for only few weeks. Although a conditioned medium of primary-cultured astrocytes can be effective in culturing neurons for a longer period of time, the use of primary astrocytes may not be practical due to a number of limitations, including restricted availability of neural tissues as source of astrocytes, and extensive time and effort to obtain astrocytes from living tissues. Additionally, it is very difficult to maintain a stable culture of primary cells in a culture vessel, and subculture of these cells is limited within few passages.

The properties of primary-cultured astrocytes vary depending on the maturation stage of the living body and the region of the living tissue from which the astrocytes are derived. In addition, when astrocytes are obtained from a living body, contamination with cells other than the desired astrocytes is inevitable. Thus, it is difficult to prepare a stable astrocyte-conditioned medium having substantially uniform quality. With our method, on the other hand, ES-ACM can efficiently induce differentiation of hES cells into neural cells. Moreover, large amounts of ES-ACM can be produced stably and readily. ES-ACM, like P-ACM, can keep neuron cultures stable for more than eight weeks until mature neuronal phenotypes are apparent. In addition, completely xeno-free ES-ACM can be generated from immature hES cells by culture in chemically defined medium. With this completely xeno-free ES-ACM, xeno-free neurons and astrocytes can repeatedly be produced. In our transplantation experiment, donor cells did not express undifferentiated markers, such as Oct-3 and SSEA-4. In addition, only few Ki-67 positive cells found in the vicinity of the grafts were hrGFP-negative. These cells were unlikely to be derived from donor cells. It is important to exclude tumorigenicity of neuronal cells derived with this xeno-free method in future

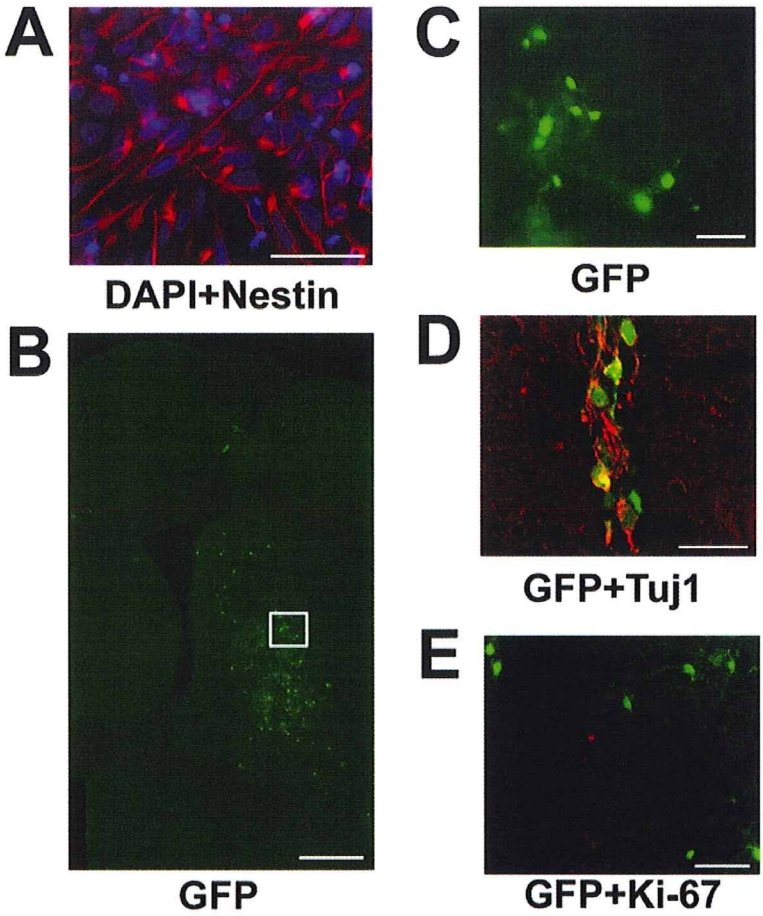

Figure 6. Survival of transplanted neural stem cells *in vivo*. (A): Most of the donor cells were confirmed to be Nestin-immunoreactve neural stem cells before transplantation. Anti-Nestin staining (green) and DAPI (blue). Bar = 50 μm. (B): Transplantation site. Grafted cells expressing hrGFP can be seen in the striatum. Bar = 500 μm. (C): High power magnification view of a white box in panel A. Some of the hrGFP-positive cells display a morphology similar to that of neurons. Bar = 50 μm. (D): Merged image of hrGFP expression (green) and immunostaining of anti-Tuj1 (red). Bar = 20 μm. (E): Merged image of hrGFP expression (green) and immunostaining of anti-Ki-67 (red). Bar = 50 μm.
doi:10.1371/journal.pone.0006318.g006

study for application to the cell therapy. Further studies are necessary to identify the specific molecules that induce neural cells in P- and ES-ACMs.

Recently, two methods adopting human tissue-derived cells have been reported as appropriate for clinical applications. One is an improved stromal cell-induced method that uses an amniotic membrane matrix [12]. The other uses telomerase-immortalized midbrain astrocytes [13]. Although both methods are xeno-free, they still need primary human tissues. On the other hand, with our method, neural cells can be induced from ES cells themselves. This self-serving method can supply donor cells consistently and may have an advantage for clinical applications.

Materials and Methods

ES cell culture

All experiments using hES cells were performed in conformity with "The Guidelines for Derivation and Utilization of Human Embryonic Stem Cells" of the Japanese government after approval by the institutional review board of Mitsubishi Tanabe Pharma Corporation. Two hES cell lines, SA002 and SA181, were obtained from Cellartis AB (Goteborg, Sweden) [14] and maintained on a mitotically inactivated mouse embryonic fibroblast feeder layer in a culture medium (vitroHES, Vitrolife AB, Goteborg, Sweden), supplemented with 4 ng/ml FGF-2 (Invitrogen, Carlsbad, CA). For passaging, the hES cells were treated with collagenase type IV (200 U/ml; Invitrogen) for 5 min, gently scraped from the culture dish, and then split 1:2–1:4 onto a feeder layer of mouse embryonic fibroblasts inactivated with 10 μg/ml mitomycin C.

Electroporation

All recombinant DNA experiments conformed to National Institute of Health (NIH) guidelines. First, a pGFP plasmid, in which hrGFP (Stratagene, La Jolla, CA) was expressed under the control of a CAG promoter (a gift from J. Miyazaki) [15] was constructed. Ten micrograms of the linearized plasmid was then electroporated into a suspension of hES cells (10^7 cells) in 0.8 mL of PBS using a Gene Pulser (500 μF, 250 V, Bio-Rad, Hercules, CA). The cells were next incubated on ice for 10 minutes, plated, and allowed to recover for 24 hours before selection with G418 (200 μg/mL). The cells were daily fed with the culture medium containing G418 for 12 days, after which the resulting ten G418-

resistant ES colonies showing strong hrGFP expression were individually picked and propagated. To analyze stem cell markers, alkaline phosphatase activity and cell surface markers were detected using an ES cell characterization kit (Chemicon, Temecula).

hES cell differentiation

Whole colonies of undifferentiated hES cells, 800–1000 μm in diameter, were picked up from the feeder layer using a glass capillary and transferred into non-adhesive bacteriological dishes each containing P-ACM supplemented with 20 ng/ml FGF-2 (R&D Systems Inc., Minneapolis). P-ACM was prepared as described previously [7]. The colonies were then cultured for 12 days, giving rise to spheres, which were next plated onto poly-L-Lysine/Laminin (Sigma-Aldrich, St. Louis) coated dishes and cultivated for seven days in NSCM (Neurobasal medium supplied with B27 supplement, both from Invitrogen, 20 ng/ml FGF-2, and 20 ng/ml recombinant EGF [R&D systems]). At this stage, the spheres gave rise to circular clusters of cells, many of which migrated from the clusters to the surrounding areas. After replacing the NSCM with P-ACM and culture for 14 days, the spheres differentiated into neurons and few astrocytes. To obtain more and purer neurons, the centers of the clusters containing undifferentiated ES cells were removed with a glass capillary, and the rest of the clusters were cultured for seven days in NSCM. Neuronal differentiation was then induced by subculture of neural stem cells using 0.05% Trypsin/EDTA in P-ACM for 14 days. To induce astrocytic differentiation, the neural stem cells were subcultured in G5 medium (Neurobasal medium supplemented with G5 supplement, both from Invitrogen, 10 ng/ml FGF-2, and 20 ng/ml EGF) for 14 days.

To induce astrocytic differentiation under xeno-free conditions, the colonies of hES cells were transferred into non-adhesive bacteriological dishes each containing N2 medium (Neurobasal medium supplied with N2 supplement, Invitrogen) supplemented with 20 ng/ml of FGF-2 and EGF. After the colonies were cultured for 12 days, few of them gave rise to spheres containing neural stem cells, which were subsequently plated onto poly-L-Lysine/Laminin in G5 medium. Centers of the spheres containing undifferentiated hES cells were removed with a glass capillary, and the rest of the clusters were cultured for seven days in G5 medium. By repeating over this cycle eight times, the spheres were purified to obtain pure neural stem cells. These neural stem cells were subcultured in G5 medium for 14 days to induce astrocytes. For collection of ES-ACM, hES cells derived-astrocytes were cultured in N2 medium for two days.

Immunostaining analysis

hES cells cultured in a 24-well plate were fixed in 4% paraformaldehyde in phosphate-buffered saline (PBS). Immunocytochemistry was performed using standard protocols and antibodies directed against Tuj1 (monoclonal 1:1000), MAP2 (monoclonal, 1:1000), GFAP (polyclonal 1:500), Oct-4 (monoclonal 1:500), SSEA-4 (monoclonal 1:400), Nestin (monoclonal 1:1000) (all from Chemicon), and TH (monoclonal, 1:400) (Acris Antibodies, Hiddenhausen, Germany). Alexa Fluor 594-labeled (Molecular Probes, Eugene, OR) and Cy3-labeled (GE healthcare, Uppsala, Sweden) secondary antibodies were used for visualization. 4′, 6-diamidino-2-phenylindole (DAPI, Kirkegaard Perry Laboratories, Gaithersburg) was used for nuclei staining.

Cell density of neural lineages (neurons and astrocytes) was determined by counting the numbers of DAPI, Tuj^+ and $GFAP^+$ cells per field at a magnification of 200 times using an inverted microscope. Five visual fields were randomly selected and counted for each sample. Numbers presented in figures represent the average percentage and SEM of positive cells over DAPI from three samples per each examination.

RT-PCR analysis

Total RNA was extracted from undifferentiated hES cells, neural stem cells, and neuronal cells using QIAshredder (QIAGEN, Hilden, Germany) and RNeasy Plus Mini kit (QIAGEN). Reverse transcription was carried out using random hexamers at 37°C for 60 minutes according to the manufacturer's instruction for First-Strand cDNA Synthesis Kit (GE Healthcare UK Ltd., Buckinghamshire, UK). PCR was carried out for 30 cycles using the specific primer sets. The reaction cycle was set at 95°C for 30 seconds, 55°C for 30 seconds, and 72°C for 30 seconds. The amplified fragments were subjected to electrophoresis in a 2% agarose gel, which was subsequently stained with ethidium bromide and photographed. The primers used are as follows: glyceraldelyde-3-phosphatedehydrogenase (GAPDH), ACCACAGTCCATGCCATCAC and TCCACCACCCTGTTGCTGTA; Oct4, CGTTCTCTTTGGAAAGGTGTTC and ACACTCGGACCACGTCTTTC; Nanog, AAGACAAGGTCCCGGTCAAG and CCTAGTGGTCTGCTGTATTAC; MAP2, CTTTCCGTTCATCTGCCATT and GCATATGCGCTGATTCTTCA; Nurr1, GCTAAACAAAACTTGCATGC and CTCATATCATGTGCCATACTAG; TH, GAGTACACCGCCGAGGAGATTG and GCGGATATACTGGGTGCACTGG; choline acetyltransferase (ChAT), ATGGGGCTGAGGACAGCGAAG and AAGTGTCGCATGCACTGCAGG; glutamic acid decarboxylase (GAD), ATTCTTGAAGCCAAACAG and TAGCTTTTCCCGTCGTTG.

Electrophysiology

The action potential was recorded using current clamp mode of Axopatch200B amplifier and Digidata 1320 interface (Axon, CA, USA). Physiological bathing solution contained (in mM); 140 NaCl, 5.4 KCl, 0.33 NaH_2PO_4, 0.5 $MgCl_2$, 1.8 $CaCl_2$, 5 HEPES (pH = 7.4 with NaOH). Standard high K^+ pipette solution contained; 110 Aspartic acid, 30 KCl, 5 MgATP, 5 Na_2 creatine phosphate, 0.1 Na_2GTP, 2 EGTA, 10 HEPES (pH = 7.2 with KOH). Electrode resistance was 8~6 MOhm. All experiments were carried out at 33–35°C.

Transplantation Experiment

Neural stem cells derived from hES cells using ES-ACM were implanted into the mouse striatum. All animal experimental protocols were approved by the Animal Ethics Committee of Mitsubishi Tanabe Pharma Corporation. 8-week-old C57BL/6 Cr Slc mice (SLC, Shizuoka, Japan) were anesthetized with pentobarbital and fixed on a stereotactic device (Narishige, Tokyo, Japan). By using a glass pipette with an inner diameter of 100 μm, 1×10^5 cells/5 μl were slowly (0.3 μl/min) injected into the striatum (AP±0 mm, ML +2.0 mm, DV −3.0 mm from bregma) of an adult male mouse. Four weeks after the transplantation, the recipient mouse was anesthetized with pentobarbital and perfused with ice-cold 4% paraformaldehyde in PBS. The brains of each mouse were postfixed in the same solution, cryoprotected with 30% sucrose in PBS for 48 h, and frozen. Coronal sections (thickness 40 μm) were cut on a microtome with freezing unit, collected in PBS (pH 7.4), and divided into series. Brain sections were incubated overnight with primary antibodies at 4°C. The primary antibodies used for immunohistochemistry ware mouse anti-Tuj1 (1:800, Covance, USA) and rabbit anti-Ki67 (1:25, abcam, UK). For detection of the primary antibodies, Alexa Fluor 594 goat anti-mouse IgG (1:1000; Molecular Probes) and Alexa

Fluor 594 goat anti-rabbit IgG (1:1000; Molecular Probes) were incubated with the samples. Immunoreactivity was assessed and viewed under confocal laser scanning microscopy (FV10i; Olympus, Tokyo).

Acknowledgements

We thank Jun-ichi Miyazaki, Osaka University Medical School, Osaka, Japan for the generous gift of plasmid pCAG. We also thank Naomi Takino and Hiroko Nishida, Division of Neurology, Department of Medicine, Jichi Medical University, Tochigi, Japan, for their technical assistance.

Author Contributions

Conceived and designed the experiments: TO HM SiM YK. Performed the experiments: TO NK HM KW MT. Analyzed the data: TO HM YS SN TI IN SiM MT YK. Contributed reagents/materials/analysis tools: TN SiM MT NI. Wrote the paper: TO SiM MT YK.

References

1. Thomson JA, Itskovitz-Eldor J, Shapiro SS, Waknitz MA, Swiergiel JJ, et al. (1998) Embryonic stem cell lines derived from human blastocysts. Science 282: 1145–1147.
2. Suemori H, Tada T, Torii R, Hosoi Y, Kobayashi K, et al. (2001) Establishment of embryonic stem cell lines from cynomolgus monkey blastocysts produced by IVF or ICSI. Dev Dyn 222: 273–279.
3. Bain G, Kitchens D, Yao M, Huettner JE, Gottlieb DI (1995) Embryonic stem cells express neuronal properties in vitro. Dev Biol 168: 342–357.
4. Okabe S, Forsberg-Nilsson K, Spiro AC, Segal M, McKay RD (1996) Development of neuronal precursor cells and functional postmitotic neurons from embryonic stem cells in vitro. Mech Dev 59: 89–102.
5. Kawasaki H, Mizuseki K, Nishikawa S, Kaneko S, Kuwana Y, et al. (2000) Induction of midbrain dopaminergic neurons from ES cells by stromal cell-derived inducing activity. Neuron 28: 31–40.
6. Tropepe V, Hitoshi S, Sirard C, Mak TW, Rossant J, et al. (2001) Direct neural fate specification from embryonic stem cells: a primitive mammalian neural stem cell stage acquired through a default mechanism. Neuron 30: 65–78.
7. Nakayama T, Momoki-Soga T, Inoue N (2003) Astrocyte-derived factors instruct differentiation of embryonic stem cells into neurons. Neurosci Res 46: 241–249.
8. Nakayama T, Momoki-Soga T, Yamaguchi K, Inoue N (2004) Efficient production of neural stem cells and neurons from embryonic stem cells. Neuroreport 15: 487–491.
9. Nakayama T, Sai T, Otsu M, Momoki-Soga T, Inoue N (2006) Astrocytogenesis of embryonic stem-cell-derived neural stem cells: Default differentiation. Neuroreport 17: 1519–1523.
10. Bottenstein JE, Sato GH (1979) Growth of a rat neuroblastoma cell line in serum-free supplemented medium. Proc Natl Acad Sci U S A 76: 514–517.
11. Brewer GJ, Cotman CW (1989) Survival and growth of hippocampal neurons in defined medium at low density: advantages of a sandwich culture technique or low oxygen. Brain Res 494: 65–74.
12. Ueno M, Matsumura M, Watanabe K, Nakamura T, Osakada F, et al. (2006) Neural conversion of ES cells by an inductive activity on human amniotic membrane matrix. Proc Natl Acad Sci U S A 103: 9554–9559.
13. Roy NS, Cleren C, Singh SK, Yang L, Beal MF, et al. (2006) Functional engraftment of human ES cell-derived dopaminergic neurons enriched by coculture with telomerase-immortalized midbrain astrocytes. Nat Med 12: 1259–1268.
14. Heins N, Englund MC, Sjoblom C, Dahl U, Tonning A, et al. (2004) Derivation, characterization, and differentiation of human embryonic stem cells. Stem Cells 22: 367–376.
15. Niwa H, Yamamura K, Miyazaki J (1991) Efficient selection for high-expression transfectants with a novel eukaryotic vector. Gene 108: 193–199.

Short Report

A convenient enzyme-linked immunosorbent assay for rapid screening of anti-adeno-associated virus neutralizing antibodies

Tetsuo Ito[1], Shigekazu Yamamoto[1], Tsukasa Hayashi[1], Mika Kodera[1,3], Hiroaki Mizukami[2], Keiya Ozawa[2] and Shin-ichi Muramatsu[3]

[1]KAINOS Laboratories Inc., Tokyo; [2]Division of Genetic Therapeutics; [3]Division of Neurology, Jichi Medical University, Tochigi, Japan
Corresponding author: Shin-ichi Muramatsu, 3311-1 Yakushiji, Shimotsuke, Tochigi 329-0498, Japan. Email: muramats@jichi.ac.jp

Abstract

Background: Recombinant adeno-associated virus vectors based on serotype 2 (AAV-2) have become leading vehicles for gene therapy. Most humans in the general population have anti-AAV-2 antibodies as a result of naturally acquired infections. Pre-existing immunity to AAV-2 might affect the functional and safety consequences of AAV-2 vector-mediated gene transfer in clinical applications.

Methods: An enzyme-linked immunosorbent assay (ELISA) method was developed using microwell plates coated with intact particles of recombinant AAV-2 vectors, and horseradish peroxidase-conjugated anti-human immunoglobulin G (HRP-IgG). Neutralizing antibody titres were analysed by assessing the ability of serum antibody to inhibit transduction into HEK293 cells of AAV vectors that express β-galactosidase.

Results: Anti-AAV-2 antibodies were detected by ELISA in two of 20 healthy subjects. The positivity criterion (optical density >0.5) in ELISA corresponded to the cut-off value (320-fold dilution of serum) in the AAV-2 neutralization assay. Influences of interfering substances were not observed.

Conclusion: This ELISA method may be useful for rapid screening of anti-AAV-2 neutralizing antibodies in candidates for gene therapy.

Ann Clin Biochem 2009; **46**: 508–510. DOI: 10.1258/acb.2009.009077

Introduction

Adeno-associated virus (AAV) is a small single-stranded DNA virus within the parvovirus family.[1,2] Among more than 100 genotypes of primate AAV, serotype 2 (AAV-2) is the most studied and was the first to be engineered for vector development. Recombinant AAV-2 vectors efficiently transduce both dividing and non-dividing cells and provide long-term gene expression without significant toxicity. Growing numbers of clinical trials have been conducted using AAV-2 vectors to combat various diseases. However, one major problem is the high prevalence of anti-AAV-2 antibodies in the human population. More than 90% of adults demonstrate antibodies that cross-react with one or more AAV serotypes, although markedly fewer (18–32%) show neutralizing antibodies (nAb).[3,4] Pre-existing immunity to AAV-2 may block transduction and intensify the innate response to vector administration, leading to a poor outcome of gene therapy. Thus, measurement of the anti-AAV-2 nAb titre is necessary.

Methods

Recombinant AAV-2 vectors were produced by the triple transduction method as described previously.[5] In brief, HEK293 cells were transfected with the following three plasmids: pAAV2-Rep/vp (containing the AAV-2 *rep* and *cap* genes), pAd (containing the adenovirus genome) and pW1 (containing the β-galactosidase-expression cassette). After three days of incubation, the transfected cells were frozen and thawed, and the recombinant AAV-2 vector particles that were released were purified by two sequential CsCl density gradient centrifugations.

Serum samples from healthy adults were purchased from Advanced BioServices LLC, (Reseda, CA, USA). AAV-specific antibodies were detected using an enzyme-linked immunosorbent assay (ELISA). Ninety-six-well microtitre plates (Invitrogen, Carlsbad, CA, USA) were coated with 0.5 μg (1.4×10^8 vector genomes [vg]) of AAV-2 vector particles per well. After blocking with 2% bovine serum albumin (BSA) in phosphate-buffered saline (PBS), the plates were washed with 2% sucrose. Serum samples diluted at 1:1000 with PBS/0.1% BSA were added to each well (100 μL/well). The plates were incubated for 1 h at room temperature (RT) and washed three times with PBS/0.05% Tween 20. A solution containing 1 μg/mL horseradish peroxidase-conjugated anti-human immunoglobulin G (HRP-IgG; self-prepared using a heterobifunctional

reagent) was added to each well (100 μL/well). The plates were incubated for 1 h at RT and washed three times with washing buffer. Colour was developed by adding 100 μL 3,3′,5,5′-tetramethylbenzidine/urea hydrogen peroxide (Neogen, Lexington, KY, USA) and incubating the plates for 30 min at RT. Colour development was stopped by adding 1 mol/L sulphuric acid (100 μL/well), and the optical density (OD) was measured at 450/640 nm. The optimum reaction conditions were determined in the following ranges: 0.5×10^8 to 3×10^8 vg of AAV-2 vector particles per well, 10- to 5000-fold dilution of the specimen and 0.01–0.4 μg/mL concentration of HRP-IgG. The effects of bilirubin, haemoglobin and chyle as endogenous interference materials were studied. Samples including these materials at 500 mg/L, 5000 mg/L and 3000°, respectively, were mixed with sera at a volume ratio of 1 : 9 and analysed by ELISA.

For the nAb assay, sera were continuously diluted two-fold with Dulbecco's Modified Eagle's Medium and Harn's F-12 Nutrient Mixture (DMEM/F12, Invitrogen) 10% fetal bovine serum (Sigma-Aldrich, St. Louis, MO, USA), 100 U/mL penicillin (Invitrogen) and 100 μg/mL streptomycin (Invitrogen). AAV-2 vectors were diluted with 10 mmol/L HEPES/130 mmol/L NaCl (pH 8.0) up to 1.4×10^8 vg/μL, and optimum transduction was obtained with 1.4×10^{10} vg/μL. Ten microlitres of diluted serum were added to 5 μL diluted AAV-2 vector, and the mixture was incubated for 1 h at RT. The mixture was then added to 96-well plates containing confluent HEK293 cells. Two days after transduction, β-galactosidase activity was measured with a β-galactosidase assay kit (Invitrogen). The titre of nAb was defined as the highest dilution of serum that showed <50% of the β-galactosidase activity of the negative control.

Results and discussion

In the ELISA method developed in this study, AAV-2 vector particles immobilized on plates captured AAV-2-specific antibodies. Using whole vector particles as antigens without degradation, antibodies that are more specific AAV-2, including nAb, can be assessed. Intra-assay precision was determined by repeatedly ($n = 8$) measuring four kinds of serum with different nAb titres. For three samples whose nAb titres were ×640, ×80 and ×80, the coefficient of variation (CV) of the OD was 2.5%, 4.3% and 1.8%, respectively. For the fourth sample, with ×10 titre, the average OD was 0.012 and the CV was 8.5%. These data confirm the good precision of the assay. The effects of interference materials were <10%, suggesting that the method had good specificity. All reagents, including AAV particles, were stable after storage for 13 months at 4°C, and sensitivity of the ELISA was maintained at 95% with fresh reagents.

The nAb titres for 20 healthy donor samples varied from ×10 to ×640, and 13 samples had a titre less than ×20. Using the ELISA method, the absorbance values of the samples varied from 0.012 to 0.752, and 15 samples showed absorbance of less than 0.08 (Table 1). In our study, a nAb titre higher than × 32 corresponded to an OD greater than 0.5 in the ELISA. If these values were used as cut-off points, two of 20 samples found to be positive in both the nAb assay and the ELISA. Further studies on more samples were necessary to validate the cut-off values in different populations.

Table 1 Correlation between a neutralizing antibody assay (nAb) and the ELISA method

	nAb assay		ELISA	
Sample ID	nAb titre	Decision	OD	Decision
1	10	Neg.	0.014	Neg.
2	80	Neg.	0.075	Neg.
3	10	Neg.	0.013	Neg.
4	10	Neg.	0.016	Neg.
5	160	Neg.	0.291	Neg.
6	80	Neg.	0.015	Neg.
7	80	Neg.	0.032	Neg.
8	10	Neg.	0.010	Neg.
9	10	Neg.	0.025	Neg.
10	10	Neg.	0.012	Neg.
11	10	Neg.	0.014	Neg.
12	80	Neg.	0.468	Neg.
13	10	Neg.	0.012	Neg.
14	320	Pos.	0.596	Pos.
15	640	Pos.	0.725	Pos.
16	10	Neg.	0.013	Neg.
17	20	Neg.	0.114	Neg.
18	10	Neg.	0.046	Neg.
19	10	Neg.	0.016	Neg.
20	10	Neg.	0.012	Neg.

OD, optical density; ELISA, enzyme-linked immunosorbent assay; nAb, neutralizing antibodies

AAV-2 antibody in 20 sera from healthy individuals was analysed by ELISA and a neutralizing antibody assay. The measured values were expressed as OD or titre. The cut-off value for the neutralizing antibody assay was provisionally fixed at ×320. The criterion for positivity for the ELISA method was considered greater than OD 0.5

Conclusion

We have developed a simple and convenient ELISA method for detecting serum anti-AAV-2 antibodies. Antibody titres assessed by this method show good correlation with nAb titres obtained in a cell transduction assay, suggesting that this ELISA may be useful for the rapid screening of nAbs in candidates for gene therapy.

DECLARATIONS

Competing interests: None.

Funding: Part of this work was supported by a grant (19591003) from the Ministry of Education, Science, Sports and Culture of the Japanese Government, and a grant (20261501) from the Japan Ministry of Health, Labour and Welfare.

Ethical approval: The ethics committee of Jichi Medical University approved this study (GT-001).

Guarantor: SM.

Contributorship: Conceived and designed the experiments: SM, HM, TI, TH. Performed the experiments: TY, MK, HM, Analysed the data: TI, SY, TH, MK, HM, KO, SM, Wrote the paper: TI, SM.

REFERENCES

1 Gao G, Vandenberghe LH, Alvira MR, *et al.* Clades of adeno-associated viruses are widely disseminated in human tissues. *J Virol* 2004;**78**:6381–8
2 Wu Z, Asokan A, Samulski RJ. Adeno-associated virus serotypes: vector toolkit for human gene therapy. *Mol Ther* 2006;**14**:316–27
3 Chirmule N, Propert K, Magosin S, *et al.* Immune responses to adenovirus and adeno-associated virus in humans. *Gene Ther* 1999;**6**:1574–83
4 Moskalenko M, Chen L, van Roey M, *et al.* Epitope mapping of human anti-adeno-associated virus type 2 neutralizing antibodies: implications for gene therapy and virus structure. *J Virol* 2000;**74**:1761–6
5 Li XG, Okada T, Kodera M, *et al.* Viral-mediated temporally controlled dopamine production in a rat model of Parkinson disease. *Mol Ther* 2006;**13**:160–6

(Accepted 24 June 2009)

Development/Plasticity/Repair

Nurr1 Is Required for Maintenance of Maturing and Adult Midbrain Dopamine Neurons

Banafsheh Kadkhodaei,[1] Takehito Ito,[2] Eliza Joodmardi,[1] Bengt Mattsson,[3] Claude Rouillard,[1] Manolo Carta,[3] Shin-Ichi Muramatsu,[4] Chiho Sumi-Ichinose,[5] Takahide Nomura,[5] Daniel Metzger,[6] Pierre Chambon,[6] Eva Lindqvist,[7] Nils-Göran Larsson,[8,10] Lars Olson,[7] Anders Björklund,[3] Hiroshi Ichinose,[2] and Thomas Perlmann[1,9]

[1]Ludwig Institute for Cancer Research, Stockholm Branch, SE-171 77 Stockholm, Sweden, [2]Graduate School of Bioscience and Biotechnology, Tokyo Institute of Technology, Yokohama 226-8501, Japan, [3]Wallenberg Neuroscience Center, Lund University, SE-221 84 Lund, Sweden, [4]Department of Neurology, Jichi Medical University, Tochigi 329-0498, Japan, [5]Department of Pharmacology, Fujita Health University School of Medicine, Toyoake, Aichi 470-1192, Japan, [6]Department of Functional Genomics Institut de Génétique et Biologie Moléculaire et Cellulaire, 67404 Illkirch, France, Departments of [7]Neuroscience, [8]Laboratory Medicine, and [9]Cell and Molecular Biology, Karolinska Institutet, SE-171 77 Stockholm, Sweden, and [10]Max Planck Institute for Biology of Ageing, D-50931 Cologne, Germany

Transcription factors involved in the specification and differentiation of neurons often continue to be expressed in the adult brain, but remarkably little is known about their late functions. Nurr1, one such transcription factor, is essential for early differentiation of midbrain dopamine (mDA) neurons but continues to be expressed into adulthood. In Parkinson's disease, Nurr1 expression is diminished and mutations in the *Nurr1* gene have been identified in rare cases of disease; however, the significance of these observations remains unclear. Here, a mouse strain for conditional targeting of the *Nurr1* gene was generated, and *Nurr1* was ablated either at late stages of mDA neuron development by crossing with mice carrying Cre under control of the dopamine transporter locus or in the adult brain by transduction of adeno-associated virus Cre-encoding vectors. *Nurr1* deficiency in maturing mDA neurons resulted in rapid loss of striatal DA, loss of mDA neuron markers, and neuron degeneration. In contrast, a more slowly progressing loss of striatal DA and mDA neuron markers was observed after ablation in the adult brain. As in Parkinson's disease, neurons of the substantia nigra compacta were more vulnerable than cells in the ventral tegmental area when *Nurr1* was ablated at late embryogenesis. The results show that developmental pathways play key roles for the maintenance of terminally differentiated neurons and suggest that disrupted function of Nurr1 and other developmental transcription factors may contribute to neurodegenerative disease.

Introduction

Adaptation to a changing environment requires plasticity in the adult CNS. However, to ensure that neurons are properly maintained, such plasticity must be balanced against mechanisms that counteract phenotypic instability. Studies of how neurons develop may help to unravel functions important for the stability of nerve cells as factors promoting their differentiation may also contribute to their maintenance. Indeed, many transcription factors identified for their critical roles during neuronal development continue to be expressed in the postnatal nervous system, raising the possibility that they contribute to the integrity of already differentiated neurons (Hendricks et al., 1999; Vult von Steyern et al., 1999; Kang et al., 2007; Alavian et al., 2008). However, the consequences of adult gene ablation of any of these factors have not yet been reported, and very little is known of their functions in differentiated neurons.

From a clinical perspective, it is of particular interest to identify factors that maintain stability of neurons that are affected in neurodegenerative disorders as loss of phenotype would likely cause or contribute to disease. Parkinson's disease (PD) is characterized by progressive pathology of midbrain dopamine (mDA) neurons of substantia nigra pars compacta (SNc) and the ventral tegmental area (VTA), typically involving deposition of α-synuclein-rich cytoplasmic protein aggregates termed Lewy bodies. During development, early signaling events induce transcription factors that control the specification and differentiation of mDA neurons (Smidt and Burbach, 2007). Several of these factors, including Nurr1, Lmx1a, Lmx1b, Pitx3, FoxA2, and En1/2, continue to be expressed in the postnatal and adult brain (Zetterström et al., 1996; Smidt et al., 1997, 2000; Albéri et al., 2004; Simon et al., 2004; Kittappa et al., 2007). Nurr1, belonging to a family of ligand-independent nuclear receptors (Wang et al.,

Received Aug. 11, 2009; revised Oct. 17, 2009; accepted Oct. 28, 2009.

This work was supported by grants from the Michael J. Fox Foundation (T.P., A.B., L.O.), Vetenskapsrådet via Linné Center DBRM (T.P.), Grants-in-Aid for Human Frontier Science Program (P.C., D.M., H.I.), Grants-in-Aid for Scientific Research from the Ministry of Education, Culture, Sports, Science, and Technology of Japan, the Ministry of Health, Labor, and Welfare of Japan, and the Japan Science and Technology Agency, Core Research for Evolutional Science and Technology (S.-I.M., H.I.), Vetenskapsrådet (L.O.), Swedish Brain Power (L.O.), Swedish Brain Foundation (L.O.), and the Swedish Parkinson Foundatin (L.O.). We are grateful to Johan Ericson and members of the Perlmann and Ericson laboratories for valuable discussions. We thank Andrée Dierich and Jean-Marc Bornert for their help in mouse mutagenesis, Noriko Ihira for help in construction of the targeting vector and screening of ES clones, Björn Anzelius and Naomi Takino for their help with AAV vectors, Ulla Jarl for help with histology, and Marie-Louise Alun for advice on mice handling.

Correspondence should be addressed to either of the following: Thomas Perlmann, Department of Cell and Molecular Biology, Karolinska Institutet, SE-171 77 Stockholm, Sweden, E-mail: thomas.perlmann@licr.ki.se; or Hiroshi Ichinose, Graduate School of Bioscience and Biotechnology, Tokyo Institute of Technology, Yokohama 226-8501, Japan, E-mail: hichinos@bio.titech.ac.jp.

DOI:10.1523/JNEUROSCI.3910-09.2009

 0270-6474/09/2915923-10$15.00/0

2003; Perlmann and Wallén-Mackenzie, 2004), becomes expressed in developing mDA neurons that have just exited the cell cycle and is essential for mDA neuron development because mDA neurons of both the SNc and VTA fail to express dopaminergic markers and newborn *Nurr1*-null mice lack mDA neuron cell bodies and their striatal projections (Zetterström et al., 1997; Castillo et al., 1998; Saucedo-Cardenas et al., 1998). How Nurr1 regulates target genes in mDA neuron development remains essentially unknown but may involve a functional interaction with the homeobox transcription factor Pitx3 (Jacobs et al., 2009).

Determining the role of Nurr1 also in the adult brain is of particular importance because previous studies suggested an association of this protein with PD pathology. Nurr1 expression is diminished in neurons with α-synuclein inclusions in postmortem PD brain tissue, and *Nurr1* mutations and polymorphisms have been identified in rare cases of PD (Xu et al., 2002; Le et al., 2003; Zheng et al., 2003; Grimes et al., 2006). However, the significance of genetic lesions remain unclear (Wellenbrock et al., 2003; Hering et al., 2004; Tan et al., 2004). These observations emphasize the importance of elucidating the role of Nurr1 in more mature mDA neurons by analyzing the consequences of conditional *Nurr1* gene ablation in mice.

Materials and Methods

Conditional Nurr1 gene-targeted mice. Mouse 129SV genomic library constructed in bacterial artificial chromosome (BAC) was screened by PCR. A BAC clone containing the entire Nurr1 gene was selected, and a BamHI–MunI fragment containing exon 1 to exon 5 was recloned into a pBluescript II vector. A floxed neomycin cassette was inserted into an internal EcoRI site located in intron 3, and a synthetic loxP sequence was inserted at SalI site located in intron 2. Mouse embryonic stem (ES) cells were electroporated with the targeting vector, and the homologously recombinated clones were screened by PCR and Southern blot analysis. ES clones with three loxP sites were selected, and a plasmid expressing Cre DNA recombinase was transiently transfected into the cells. ES cells with two loxP sites without a neomycin cassette were selected by PCR and used for production of chimeric mice.

Animals. Mice were kept in rooms with controlled 12 h light/dark cycles, temperature, and humidity, with food and water provided *ad libitum*. All animal experiments were performed with permission from the local animal ethics committee. The generation of dopamine transporter (*DAT*)–*Cre* mutant mice has been described previously (Ekstrand et al., 2007). Mice were mated during the night, and the females were checked for vaginal plugs in the morning [day of vaginal plug considered as embryonic day 0.5 (E0.5)].

L-3,4-Dihydroxyphenylalanine treatment. Methyl L-3,4-dihydroxyphenylalanine (L-DOPA) hydrochloride and the peripheral DOPA decarboxylase inhibitor benserazide-HCl (Sigma-Aldrich) were dissolved in Ringer's solution immediately before use. L-DOPA was intraperitoneally given every second day at the dose of 2.5 mg/kg combined with 0.625 mg/kg benserazide. Chronic treatment with L-DOPA/benserazide was administered for 50 d, starting at postnatal day 15 (P15). During this period, the mice were carefully observed and weight was measured regularly. Reported hyperactivity was observed in $cNurr1^{DATCre}$ mice when given a single higher dose of L-DOPA (25 mg/kg L-DOPA, 6.25 mg/kg benserazide).

Histological analyses. At embryo stages, embryos were fixed for 2–24 h in 4% phosphate-buffered paraformaldehyde (PFA), cryopreserved in 30% sucrose before being embedded in OCI (Sakura Finetek), and cryosectioned at a thickness of 10–20 μm onto slides (SuperFrostPlus; Menzel Gläser). For the isolation of brains for immunolabeling at P15 and onward, animals were anesthetized with Avertin (tribromoethanol; 0.5 mg/g) and perfused through the left ventricle with body-temperature PBS, followed by ice-cold 4% PFA. The brains were dissected and postfixed overnight in 4% paraformaldehyde and subsequently cryoprotected for 24–48 h in 30% sucrose at 4°C. The brains were serially sectioned on a cryostat or sliding microtome at 10–30 μm. Littermates were used in an all comparative experiments.

For immunohistochemistry, sections were preincubated for 1 h in blocking solution containing either 10% normal goat sera or 5–10% bovine serum albumin, 0.25% Triton X-100, and 0.01% Na-azide in PBS. Primary antibodies diluted in blocking solution were applied overnight at 4°C. After rinses with PBS, biotinylated- or fluorophore-conjugated secondary antibodies diluted in PBS were applied for 1 h at room temperature. Biotinylated secondary antibodies were followed by incubation with streptavidin–horseradish peroxidase complex (ABC elite kit, Vectastain) for 1 h and subsequent exposure to diaminobenzidine (DAB kit; Vector Laboratories). Primary antibodies and dilution factors were as follows: rabbit anti-Nurr1 (1:100; M196; Santa Cruz Biotechnology), anti-Nurr1 (1:250; E20; Santa Cruz Biotechnology), rabbit anti-tyrosine hydroxylase (TH) (1:500; Pel-Freeze), rat anti-DAT (1:2000; Millipore Bioscience Research Reagents), mouse anti-TH (1:200; Millipore Bioscience Research Reagents), rabbit anti-vesicular monoamine transporter (VMAT) (1:500; Millipore Bioscience Research Reagents), rabbit anti-L-DOPA decarboxylase (AADC) (1:500; Millipore Bioscience Research Reagents), rabbit anti-Cre (1:10,000; Covance Research Products), guinea pig anti-Lmx1b (1:1000) (Andersson et al., 2006), and rabbit anti-Pitx3 (Smidt et al., 2004). In some cases (anti-AADC, anti-VMAT, and anti-Nurr1), the blocking steps were performed after antigen retrieval (Dako). Finally, expression was detected by secondary antibodies from Jackson ImmunoResearch. Section images were collected by confocal microscopy (Leica DMIRE2) and bright-field microscopy (Eclipse E1000K; Nikon). Cell counting was performed by counting all SNc DA neurons detected by immunohistochemistry (DAB) in a total of three sections per animal (every 12th tissue section) within the ventral midbrain of animals taken at 4 months after vector injection in both wild-type wt^{AAVCre} and $cNurr1^{AAVCre}$ animals. The mean of counted cells per animal was established from both the injected and non-injected sides in each animal, and the relative decrease was calculated as a percentage as described in Results.

AAV–Cre injections. Two and a half- to 5-month-old animals received one unilateral stereotaxic injection in the right striatum using a 10 μl Hamilton microsyringe fitted with a glass pipette tip. The animals were anesthetized with isoflurane, 1 μl was injected during 5 min, and the cannula was left in place for an additional 2 min before being slowly retracted. The anteroposterior and mediolateral coordinates from bregma were −2.8 and −1.1 mm, respectively, and the dorsoventral coordinates from the dura were −4.3 mm. Animals were killed 0.5, 1.5, and 4 months after injection, and the brains were isolated.

Measurement of tissue content for dopamine, serotonin, and their metabolites. In supplemental Tables 1–3 (available at www.jneurosci.org as supplemental material), tissues were collected from P1, P7, P14, and adult (P48) wt^{DATCre} and $cNurr1^{DATCre}$ mice. One- to 14-d-old mice were killed by decapitation, and P48 mice were killed by cervical dislocation. Brains were rapidly removed, chilled in saline (4°C), dissected, frozen on dry ice, and stored at −80°C until use. To process tissues for HPLC and electrochemical detection of monoamines and metabolites, samples were homogenized by sonication in 5 vol or in 30 μl of 0.1 M perchloric acid, followed by centrifugation. Endogenous levels of noradrenaline, DA, 3,4-dihydroxyphenylacetic acid, homovanillic acid (HVA), serotonin (5-HT), and 5-hydroxyindoleacetic acid were determined in the supernatants. A reverse column (BAS, C-18, 100.0 × 3.2 mm, 3 μm particle diameter) was used for separation. The mobile phase consisted of 0.05 M sodium phosphate/0.03 M citric acid buffer containing 0.1 mM EDTA and was adjusted with various amounts of methanol and sodium-L-octane sulfonic acid. The flow rate was 0.3 ml/min. Monoamines and metabolites were detected using a glassy-carbon electrode detector, which as set at +0.7 V versus an Ag/AgCl reference electrode. Resultant peaks were measured and compared with repeated control samples containing fixed mixed amounts of compounds of interest.

In supplemental Table 4 (available at www.jneurosci.org as supplemental material), all animals were killed, and striata and cortex were rapidly dissected out, frozen on dry ice, and stored at −80°C. To determine monoamines, tissue was homogenized in 0.1 M perchloric acid and centrifuged at 10,000 rpm for 10 min before filtering though minispin filters for an additional 3 min at 10,000 rpm. The tissue extract were then analyzed by HPLC as described previously (Carta et al., 2007) with minor

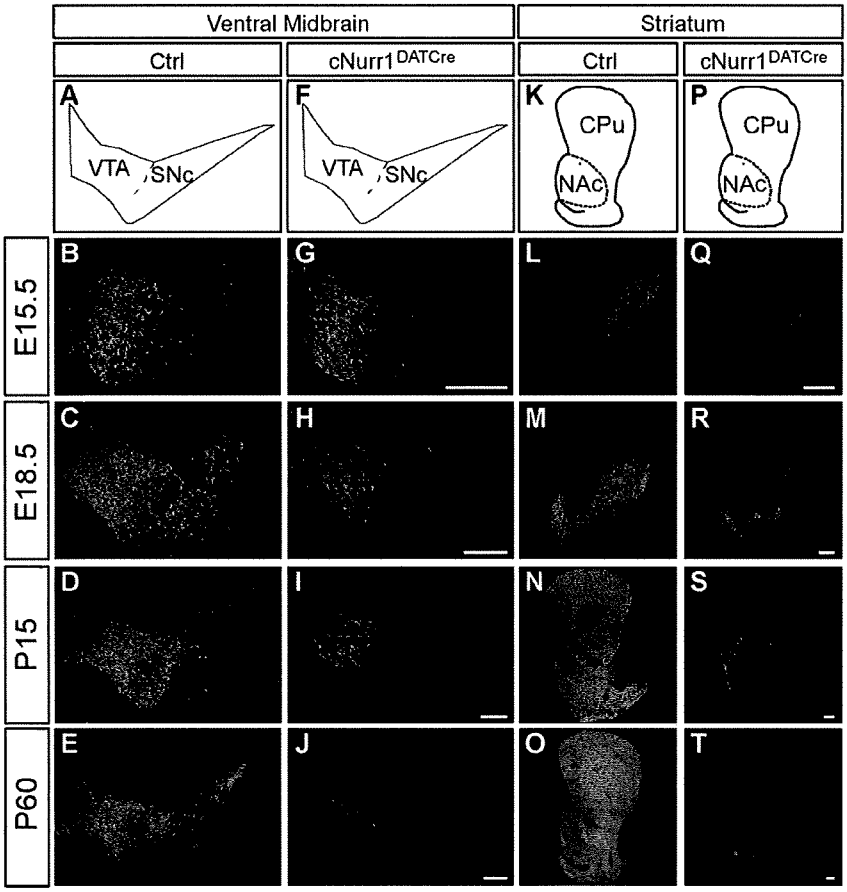

Figure 1. TH is progressively lost in both the ventral midbrain and striatum of *cNurr1*^{DATCre} mice. ***A–T***, Confocal microscopy showing TH immunohistochemistry in control (ctrl) and *cNurr1*^{DATCre} mice as indicated. ***A–J***, Sections were analyzed at the levels of ventral midbrain (as indicated in ***A*** and ***F***) and in the striatum (as indicated in ***K*** and ***P***). TH immunofluorescence was analyzed at both embryonal and postnatal stages as indicated. Results demonstrate a progressive loss of TH immunoreactivity in the ventral midbrain. Note that TH immunoreactivity was more drastically downregulated at more lateral regions compared with the prospective medial VTA. ***K–T***, TH immunoreactivity in the striatum. In *cNurr1*^{DATCre} mice, TH was lost in the CPu and diminished in the NAc. Scale bars, 250 μm.

modifications. Briefly, 25 μl of each sample were injected by a cooled autosampler (Midas) into an ESA Coulochem III coupled with an electrochemical detector. The mobile phase (5 g/L sodium acetate, 30 mg/L Na2-EDTA, 100 mg/L octane-sulfonic acid, and 10% methanol, pH 4.2) was delivered at a flow rate of 500 μl/min to a reverse-phase C18 column (4.6 mm diameter, 150 mm).

Fluorogold retrograde tracing. Animals received one unilateral stereotaxic injection in the right striatum using a 5 μl Hamilton microsyringe (22 gauge steel cannula) filled with the retrograde tracer Fluorogold (hydroxystilbamidine, 4%, Biotium). The animals were anesthetized with isoflurane, 0.5 μl was injected during 1 min, and the cannula was left in place for an additional 2 min before slowly being retracted. The anteroposterior and mediolateral coordinates from bregma were 0.27 and −2.10 mm, respectively, and the dorsoventral coordinates from the dura were −2.60 mm. Animals were killed 4 d after injection, and the brains were isolated. Fresh-frozen sections (14 μm) were cut with a cryostat and examined under a epifluorescence microscope (Eclipse E1000K; Nikon) coupled to an RTke spot camera.

Open-field test. This test was used to monitor overall activity and rearing behavior. The open field consisted of a white plastic box (55 × 35 × 30 cm) with lines (squares of 7 × 35 cm) painted on its floor. The animals were put in the center of the box, habituated for 10 min, and filmed 15 min thereafter while rearing was scored. The video recordings were used to measure the number of lines crossed during the monitoring period. A line crossing was counted when the mouse moved its whole body from one square to another.

Stepping test. Forelimb akinesia was monitored in a modified version of the stepping test, as described previously for rats (Schallert et al., 1992; Kirik et al., 1998). The test was performed three times daily over 3 consecutive days. In this test, the mouse was held firmly by the experimenter with both hindlimbs and one forelimb immobilized, and the mouse was passively moved with the free limb contacting a table surface. The number of adjusting steps, performed by the free forelimb when moved in the forehand and backhand directions, over a distance of 30 cm, was recorded. Results are presented as data collected on the third testing day.

Results

Selective *Nurr1* ablation in late developing mDA neurons

A mouse strain containing a *Nurr1* allele for conditional gene ablation was generated by insertion of two loxP sequences in the second and third introns so that the coding sequence, including the first coding exon 3, is excised by Cre-mediated recombination (supplemental Fig. 1, available at www.jneurosci.org as supplemental material). To analyze the consequences of *Nurr1* ablation at late stages of mDA neuron development, we crossed floxed *Nurr1* mice with mice carrying *Cre* inserted in the locus of the *DAT* gene (Ekstrand et al., 2007). Crosses generated *Nurr1* mice that were homozygous for the conditional targeted *Nurr1* allele and heterozygous for the *DAT–Cre* allele (*Nurr1*$^{L2/L2}$;*DAT*$^{Cre/wt}$; hereafter referred to as *cNurr1*^{DATCre} mice). Littermates of genotype *Nurr1*$^{L2/L2}$; *DAT*$^{wt/wt}$ or *Nurr1*$^{w/w}$;*DAT*$^{Cre/wt}$ were used as controls. Although we cannot exclude that a small number of cells escape Nurr1 gene deletion, immunohistochemistry using an antibody against Nurr1 showed that *DAT–Cre*-mediated *Nurr1* ablation resulted in the expected delayed loss of Nurr1 expression in mDA neurons beginning from approximately E13.5 and becomes essentially complete at E15.5 (supplemental Fig. 2, available at www.jneurosci.org as supplemental material). At this stage of normal development, cells express pan-neuronal properties as well as many mDA neuron markers, and axons are growing toward the developing striatum (Smidt and Burbach, 2007).

cNurr1^{DATCre} mice were born at the expected Mendelian frequency of ~25% (of a total n = 159); however, *cNurr1*^{DATCre} mice were less active than controls and did not survive beyond 3 weeks after birth. If litters were allowed to remain with their mothers after weaning, perinatal death was avoided in ~50% of *cNurr1*^{DATCre} pups. These surviving mice were, however, ~40% smaller than controls at the age of 2 months (supplemental Fig. 3, available at www.jneurosci.org as supplemental material). Although no significant change in spontaneous light-phase locomotor activity could be observed in adult *cNurr1*^{DATCre} mice, rearing was dramatically decreased (supplemental Fig. 3, avail-

able at www.jneurosci.org as supplemental material). L-DOPA treatment of mutant mice did not improve viability and did not induce any weight gain. Instead, *cNurr1*^{DATCre} mice display a pronounced and severe hypersensitivity to L-DOPA treatment characterized by an acute phase of hyperactivity and repetitive behaviors (including repetitive gnawing, excessive grooming, and self-injury) in all tested mutant ($n = 9$) but not in any wild-type controls ($n = 7$) (see Materials and Methods). These behaviors resemble those that have been observed in neonatal 6-hydoxydopadmine lesioned rats treated with L-DOPA (Breese et al., 2005). In conclusion, late embryonic mDA neuron-selective *Nurr1* ablation is associated with decreased weight, rearing, and viability, and mice show an altered response to L-DOPA.

Reduced levels of TH and DA in brains of *cNurr1*^{DATCre} mice

The observed abnormalities are consistent with a dopaminergic deficiency. To analyze the possible cellular basis for the phenotype, brain sections from controls and *cNurr1*^{DATCre} mice were analyzed by immunohistochemistry using an antibody against TH (Fig. 1). A progressive loss of TH immunostaining in SNc was observed in the *cNurr1*^{DATCre} mice (Fig. 1*A–J*). TH levels were significantly decreased already at E15.5, soon after Nurr1 is lost, and decreased further until adulthood when only scattered TH-positive neurons could be detected. TH was diminished also within the VTA at later stages, but a significant number of cells remained even in adult animals (Fig. 1*A–J*). These cells were counted in four nonconsecutive sections for each analyzed brain. In adult control VTA, a mean of 74.5 ± 7.1 cells per section were counted in *cNurr1*^{DATCre} mice ($n = 4$) and 499.3 ± 5.2 cells in controls ($n = 3$) (Student's t test, 4.4×10^{-7}). TH immunostaining within the caudatus putamen (CPu) was completely lost (Fig. 1*K–T*). However, weak immunoreactivity remained in nucleus accumbens (NAc) innervated preferentially by VTA neurons (Fig. 1*K–T*). We also noted the appearance of ectopic TH-positive cell bodies within the striatal parenchyma in *cNurr1*^{DATCre} mice (supplemental Fig. 4, available at www.jneurosci.org as supplemental material). These cells were more frequent in regions in which striatal TH had been most severely depleted as a consequence of Nurr1 ablation and resemble TH-positive neurons appearing in rodent and primate DA-depletion models (Huot and Parent, 2007). Decreased levels of TH immunostaining were paralleled by decreased DA levels, as measured by HPLC (supplemental Tables 1–3, available at www.jneurosci.org as supplemental material). Striatal DA was dramatically reduced to 14% of controls at P1 in *cNurr1*^{DATCre} mice and was almost completely lost by P60. An increased ratio of HVA to DA at P14 indicated increased turnover of DA in remaining cells at this stage (supplemental Table 2, available at www.jneurosci.org as supplemental material). DA was more severely decreased in CPu compared with NAc (supplemental Table 3, available at www.jneurosci.org as supplemental material). In contrast, 5-HT was significantly increased in both CPu and NAc, consistent with previous findings showing increased serotonergic innervation after striatal DA depletion (Snyder et al., 1986). Thus, a severe neurotransmitter deficiency of the mesostriatal DA system is apparent in *cNurr1*^{DATCre} mice. Together, measurements of TH immunoreactivity and DA levels demonstrate that Nurr1 is critically required for maintaining TH expression and DA synthesis from late stages of mDA neuron differentiation.

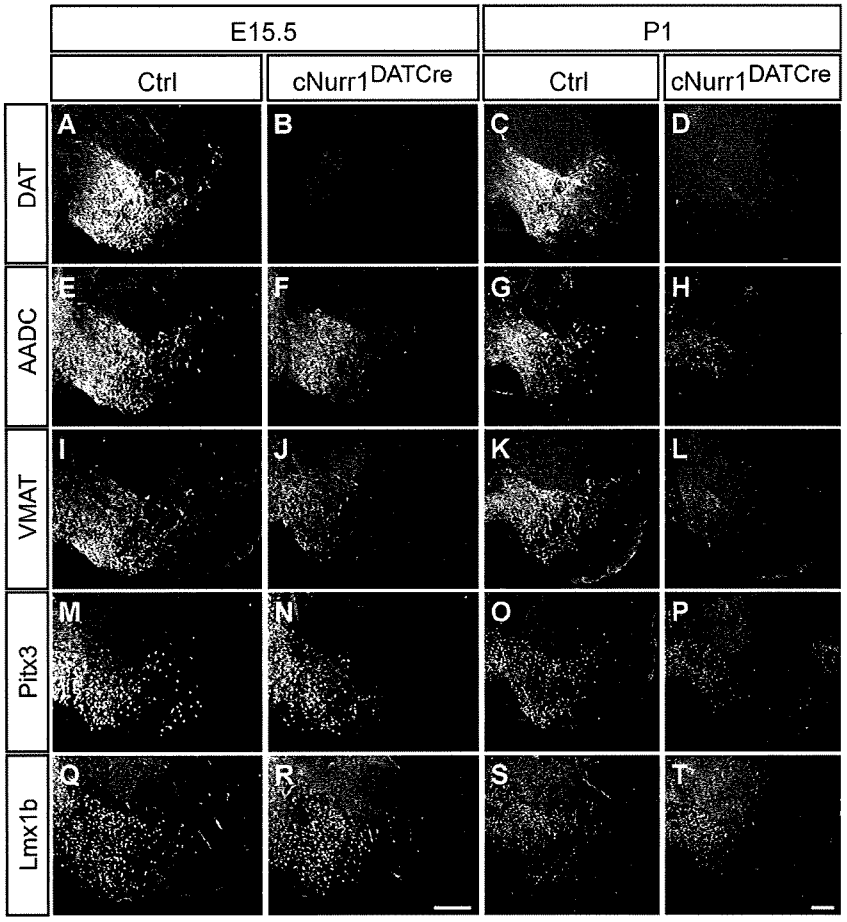

Figure 2. All analyzed mDA neuron markers are lost or diminished in *cNurr1*^{DATCre} mice. ***A–T***, Confocal microscopy showing immunohistochemistry of several different mDA neuron markers in control (ctrl) and in *cNurr1*^{DATCre} mice at E15.5 or at P1, as indicated. The following markers were analyzed: DAT, AADC, VMAT, Pitx3, and Lmx1b. Results show a progressive loss of markers that is more substantial in the lateral SNc, whereas more medial VTA cells are lost more slowly. DAT is completely absent already at E15.5 in *cNurr1*^{DATCre} mice, whereas all other markers are decreased more slowly in this area (compare ***A***, ***B***). Scale bars, 200 μm.

Cellular deficiency within the ventral midbrain of *cNurr1*^{DATCre} mice

To investigate whether the phenotype is a consequence of a more limited disruption of DA synthesis or a more severe cellular deficiency, a number of additional mDA neuron markers were analyzed. All analyzed mDA neuron markers were diminished or absent within SNc in *cNurr1*^{DATCre} mice already at E15.5 (Fig. 2). DAT was completely lost at E15.5 and therefore, consistent with previous data (Sacchetti et al., 1999), stands out as being a likely direct target of Nurr1 (Fig. 2*A–D*). Additional control experiments showed that DAT and other markers, including TH and

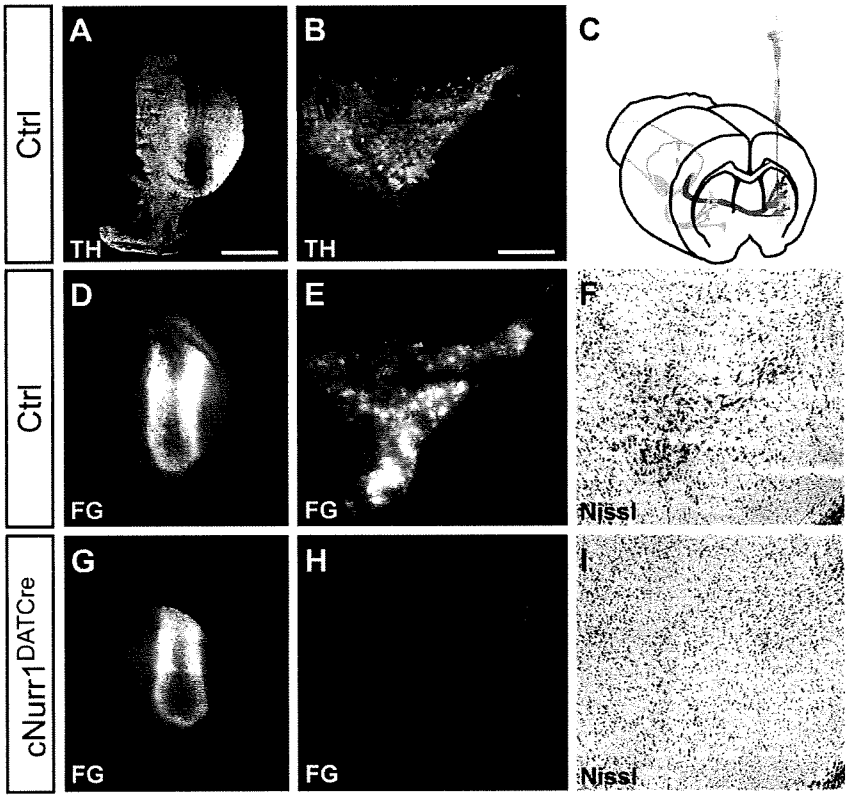

Figure 3. Cell bodies and striatal innervation are lost in $cNurr1^{DATCre}$ mice as determined by Fluorogold (FG) retrograde tracing of fibers extending from cell bodies in SNc to the striatum. ***A–C***, After Fluorogold injection, injected into the left striatum in either adult (1.5 months old) control (Ctrl) or $cNurr1^{DATCre}$ mice as indicated in ***C***, mice were killed after 4 d and analyzed for TH immunofluorescence in the striatum (***A***) or ventral midbrain (***B***). ***D–I***, Analysis for Fluorogold (FG) or by Nissl staining. Strong Fluorogold staining in both striatum (***D***) and in the ventral midbrain (***E***) was consistently seen in all control (Ctrl) animals ($n = 7$). In contrast, Fluorogold fluorescence was only detected in the striatum (***G***) in $cNurr1^{DATCre}$ mice ($n = 5$), indicating that fibers from the SNc (***H***) had been lost in these animals. Moreover, large, densely packed cell bodies are only visualized by Nissl staining in the ventral midbrain of control animals (***F***) but are completely absent from $cNurr1^{DATCre}$ mice (***I***). Striatal site of Fluorogold injection is marked by asterisk in ***A***, ***D***, and ***G***. Scale bars: ***A***, ***B***, ***D***, ***E***, ***G***, ***H***, 1 μm; ***F***, ***I***, 1200 μm.

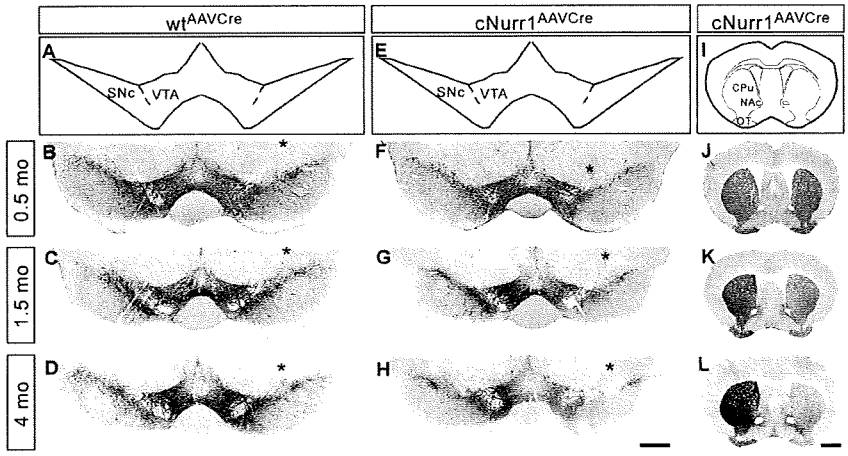

Figure 4. TH expression in both the ventral midbrain and striatum is progressively lost in the injected, but not non-injected, side of $cNurr1^{AAVCre}$ mice. ***A–H***, Sections from 0.5, 1.5, and 4 month (mo; as indicated) old AAV–Cre-injected controls (wt^{AAVCre}) or $cNurr1^{AAVCre}$ mice were used for analyses by nonfluorescent DAB TH immunostaining in the ventral midbrain. The analyzed region within the ventral midbrain is schematically illustrated in ***A*** and ***E***. The site of injection, marked by an asterisk in ***B–D*** and ***F–H***, was verified in all animals by high-power magnification microscopy and was identified as a small area of injection-induced necrosis. Results show that TH immunostaining is not drastically altered at 0.5 months but is progressively decreased at 1.5 and 4 months in the injected SNc and VTA. ***I–L***, DAB TH staining at the level of striatum. Analyzed regions are indicated in ***I***. TH staining is progressively decreased at 1.5 and 4 months in the side that is ipsilateral to the side of AAV–Cre injection in $cNurr1^{AAVCre}$ mice (***J–L***). OT, Olfactory tubercle. Scale bars: ***A–H***, 600 μm; ***I–L***, 1 mm.

Nurr1, were not visibly decreased in mice heterozygous for the *DAT–Cre* allele (supplemental Fig. 5, available at www.jneurosci.org as supplemental material) (data not shown). In contrast to DAT, AADC, VMAT2, Pitx3, or Lmx1b were not reduced within the most medial ventral midbrain at this early stage and, with the exception of DAT, markers were not completely downregulated at P1 (Fig. 2*E–T*). The progressive loss of markers indicates a severe loss of phenotype within the SNc, whereas cells within the VTA appear more resilient. Importantly, most TH-positive cells within the VTA have lost any detectable expression of DAT, indicating that these cells have not escaped Nurr1 gene targeting (supplemental Fig. 6, available at www.jneurosci.org as supplemental material).

To further assess the extent of a cellular deficiency, striatal target innervation was analyzed by Fluorogold retrograde tracing after injection into the striatum of live 8- to 9-week-old controls and $cNurr1^{DATCre}$ mice. Fluorogold was transported into SNc cell bodies of control mice; however, fluorescence was entirely undetected within the SNc of Fluorogold-injected $cNurr1^{DATCre}$ mice (Fig. 3, compare *D*, *E* with *G*, *H*). In addition, characteristic large and densely packed TH-immunoreactive mDA neurons within the SNc were virtually absent in $cNurr1^{DATCre}$ mice (Fig. 3*I*). In conclusion, Nurr1 ablation in $cNurr1^{DATCre}$ mice results in rapid loss of SNc cell bodies; however, scattered VTA neurons remained even in adult $cNurr1^{DATCre}$ mice.

Adeno-associated virus–Cre-mediated *Nurr1* ablation in adult mice

In $cNurr1^{DATCre}$ mice, *Nurr1* is ablated well before full mDA neuron maturity and before targets in the striatum have become innervated; thus, it remained possible that the phenotype is a consequence of a developmental dysfunction. Therefore, we proceeded to inactivate *Nurr1* specifically in ventral midbrain of adult mice, using an adeno-associated virus (AAV)–Cre vector driven by the neuron-specific synapsin promoter. AAV–Cre was administered by unilateral stereotaxic microinjection above the right SNc. Cre immunohistochemistry and β-galactosidase expression was analyzed after intranigral AAV–Cre injection into reporter mice in which the ROSA26 locus is targeted with a LacZ reporter gene (Soriano, 1999). Results show widespread Cre expression around the site of injection, spreading into both SNc and VTA, and robust recombination of the LacZ reporter construct (supplemental Fig. 7, available at www.jneurosci.org as supple-

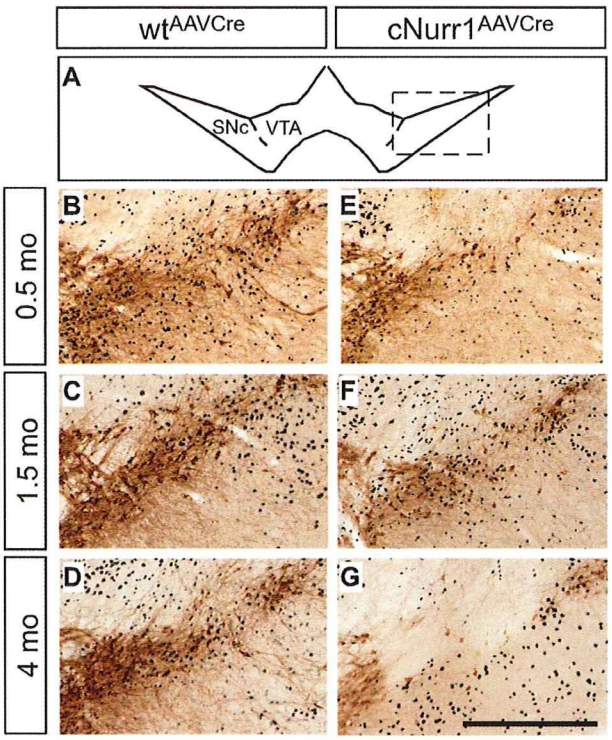

Figure 5. Cre-expressing cells are lost at 4 months within the SNc after Nurr1 ablation. ***A***, Higher magnification showing TH by DAB staining (brown) at the level of the injected SNc in wt^{AAVCre} and $cNurr1^{AAVCre}$ mice. The region that has been magnified is boxed in ***A***. ***B–G***, Adjacent sections were immunostained for Cre (black) and are superimposed on the DAB-stained TH sections in all micrographs. Cre staining is widespread in the area in which mDA neurons are normally localized at 0.5 and 1.5 months (***E***, ***F***) but almost completely absent in this area at 4 months (***G***). Scale bar, 500 μm.

mental material). Moreover, except for a small necrotic area around the site of injection, virus administration did not affect tissue morphology, expression of mDA neuron markers, or microglia activation (data not shown).

AAV–Cre was unilaterally injected above the SNc of adult mice homozygous for the floxed *Nurr1* allele to generate adult conditional gene-targeted mice ($cNurr1^{AAVCre}$) or into wild-type control mice (wt^{AAVCre}). In addition, a vector encoding the green fluorescent protein (GFP) driven by the synapsin promoter (AAV–GFP) was injected in mice homozygous for the floxed *Nurr1* allele ($cNurr1^{AAV-GFP}$ mice) to ensure that the floxed animals are not more sensitive to nonspecific toxicity induced by AAV transduction. Histological analyses were performed from animals killed at 0.5, 1.5, and 4 months after injection.

Reduction of TH and DA in adult *Nurr1*-ablated mice

TH immunohistochemistry at the level of the ventral midbrain was analyzed to assess the consequences of adult *Nurr1* ablation. Within SNc, TH immunoreactivity was unaffected at 0.5 months but was progressively reduced at 1.5 and 4 months in the injected SNc in $cNurr1^{AAVCre}$ mice (Fig. 4*E–H*). In contrast, TH immunoreactivity was unaffected in SNc of control wt^{AAVCre} and $cNurr1^{AAV-GFP}$ mice (Fig. 4*A–D*) (data not shown). TH was also reduced in the VTA at 1.5 and 4 months; however, at 4 months, the reduction in VTA was less dramatic compared with SNc (Fig. 4*E–H*).

Decreased striatal TH immunoreactivity paralleled the reduction in the ventral midbrain. Thus, although no signs of degenerating striatal TH-stained fibers (swollen axons or dystrophic neurites) were detected, striatal sections ipsilateral to the side of AAV–Cre injection showed clearly reduced TH in $cNurr1^{AAVCre}$ mice but not in controls (wt^{AAVCre} or $cNurr1^{AAV-GFP}$) (Fig. 4*I–L*) (supplemental Fig. 8, available at www.jneurosci.org as supplemental material). Diminished TH immunoreactivity was observed in regions innervated by both SNc and VTA (CPu and NAc, respectively), consistent with the reduced TH immunoreactivity in both SNc and VTA mDA neuron cell bodies. Measurement of DA and metabolites by HPLC from dissected tissue at 4 months confirmed this picture as a significant reduction in DA and DA metabolites noted both within the dorsolateral striatum and in areas mostly innervated by the VTA (cortex and ventromedial striatum) (supplemental Table 4, available at www.jneurosci.org as supplemental material). Thus, TH, DA, and DA metabolites are clearly reduced as a result of adult *Nurr1* ablation.

Loss of mDA neuron characteristics in adult *Nurr1*-ablated mice

To further analyze the fate of *Nurr1*-ablated neurons, cells were counted within the SNc and VTA in $cNurr1^{AAVCre}$ and wt^{AAVCre} mice. Within SNc, the number of TH-positive cells was significantly decreased at 4 months (58.1 ± 8.3 and 95.4 ± 6.3% in the injected vs non-injected sides of $cNurr1^{AAVCre}$ and wt^{AAVCre} mice, respectively; $p = 0.0053$). In contrast, the numbers of TH-positive cells was not significantly reduced within the VTA (104.1 ± 4.7 and 101.6 ± 10.5% in the injected versus non-injected sides of $cNurr1^{AAVCre}$ and wt^{AAVCre} mice, respectively). Also, the numbers of TH-positive cells were not significantly changed in $cNurr1^{AAVCre}$ mice at 1.5 months (data not shown).

To assess the integrity of neurons, cellular analysis was extended by analyzing Cre-immunolabeled sections that were superimposed on adjacent TH-labeled sections (Fig. 5). Notably, in $cNurr1^{AAVCre}$ mice, Cre expression was clearly detected within the area of SNc at both 0.5 and 1.5 months but was lost at 4 months in the region in which mDA neurons should normally be localized (Fig. 5, compare *E–G* with *B–D*). Cre expression is driven by a general neuronal promoter (synapsin), suggesting that loss of Nurr1 may eventually affect some pan-neuronal properties at 4 months after ablation.

Confocal microscopy confirmed the loss of TH at 1.5 and 4 months after Nurr1 ablation and the loss of Cre at 4 months (Fig. 6*A–D*). At 1.5 months, DAT expression was weak but cell bodies were readily identified (Fig. 6*E*,*F* and inset in *F*). DAT staining remained also at 4 months, but, at this stage, high-power magnification indicated that some of the staining appeared confined to fibers and/or dystrophic cells (Fig. 6*G*,*H* and inset in *H*). Nonetheless, at 4 months, most cells with decreased TH stained positive for AADC, showing that not all mDA neuron characteristics were affected (Fig. 7*A–F*). Moreover, VMAT2 is yet another marker that was severely decreased in $cNurr1^{AAVCre}$ mice, but remaining weakly stained cells were positive for the general neuronal marker Hu (Fig. 7*G–L*). The observed changes were not correlated to increased number of apoptotic cells because increased activated Caspase 3 could not be detected (data not shown). Also, we found no evidence for nigral inflammation or α-synucleinopathy because activated microglia and α-synuclein-rich inclusions were not detected at any stage after Nurr1 ablation in $cNurr1^{DATCre}$ mice (data not shown). Finally, TH and DAT expression in VTA was also affected, without any apparent loss of the neuronal marker Hu or any signs of dystrophic cells (supplemental Fig. 9, available at www.jneurosci.org as supplemental material) (data not shown). Thus, Nurr1 ablation results in a

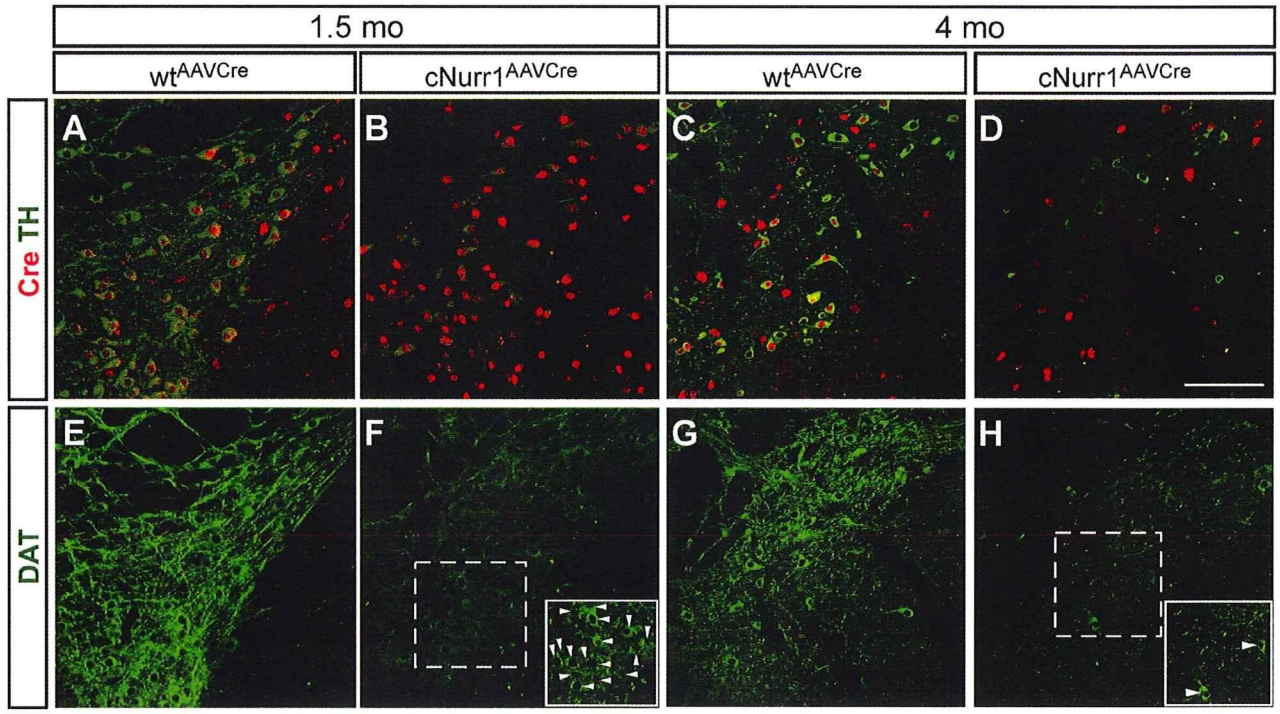

Figure 6. Decreased expression of DAT and signs of dystrophic cells in $cNurr1^{AAVCre}$ mice. ***A–H***, Confocal analysis of SNc in wt^{AAVCre} and $cNurr1^{AAVCre}$ mice at 1.5 and 4 months, as indicated. Confocal images show double staining of Cre (red) and TH (green; ***A–D***) and staining for DAT (green; ***E–H***). Micrographs show that there is a loss of TH and DAT and a progressive loss of synapsin-driven Cre at 4 months. At 4 months, DAT staining appears fragmented and stains scattered fibers, whereas very few intact cell profiles (marked with arrowheads in ***F*** and ***H***) can be identified in $cNurr1^{AAVCre}$ mice (compare insets in ***F***, ***H***). Scale bar, 200 μm.

progressive dysfunction characterized by a partial loss of the mDA neuron phenotype. Although we see few signs of neuronal degeneration, we cannot exclude a limited cell loss.

To assess whether the observed dysfunction was paralleled by an altered motor behavior, $cNurr1^{AAVCre}$ mice were subjected to a stepping test at 3 and 4 months (Schallert et al., 1992; Kirik et al., 1998). Performance of the left forelimb (i.e., the limb contralateral to the vector injection) was impaired at both time points (Fig. 8). Additional behavioral testing, including amphetamine-induced rotations and a corridor test, indicated that individual mutant animals appeared affected; however, the *Nurr1*-ablated group did not show alterations that were statistically significant (supplemental Fig. 10, available at www.jneurosci.org as supplemental material). Our results demonstrate progressive mDA neuron dysfunction, leading to a more severe deficiency at 3–4 months after *Nurr1* ablation.

Discussion

This study provides definitive evidence that Nurr1 is not only critical for early differentiation but also for the maintenance of functional mDA neurons. Conditional gene targeting at late embryogenesis, when characteristic features of mDA neurons are already apparent, results in a rapid and close to complete mDA neuron loss. Only few TH-positive cells remain within the VTA also in the absence of Nurr1. Removal of Nurr1 leads to a severe dysfunction also in adult mDA neurons. It should be noted that reduction of striatal DA and the behavioral effects after adult ablation most likely underestimate the importance of Nurr1 in the adult brain because AAV injection only transduced a proportion of all mDA neurons in the injected side of treated animals. Thus, these data emphasize the importance of studying developmental mechanisms for elucidating neuron maintenance mechanisms. An analogous example is provided by the glial cell line-derived neurotrophic factor (GDNF). GDNF is known to promote neuronal survival under development, but only recently has conditional gene targeting enabled studies that interrogate the role of GDNF and other factors signaling via Ret for maintenance of midbrain dopamine neurons in the adult brain (Oo et al., 2003; Jain et al., 2006; Kramer et al., 2007; Pascual et al., 2008).

Data presented here have implications for our understanding of how mature differentiated cell types are maintained. Previous studies have indicated that the differentiated state is not irreversible because even mature specialized cells, including for example, olfactory neurons and mature T- and B-cells, can be reprogrammed into undifferentiated pluripotent cells by either somatic cell nuclear transfer or using the recently developed methodology for the generation of induced pluripotent stem cells (Takahashi and Yamanaka, 2006; Gurdon and Melton, 2008). Nevertheless, under normal nonmanipulated conditions *in vivo*, differentiated cells are remarkably stable, indicating the importance of mechanisms that maintain cells in their appropriate differentiated state. Gene targeting in non-neural cell types has revealed how transcription factors functioning in development can be important for the maintenance of terminally differentiated cell types, e.g., Pax5 in B-lymphocytes and Prox1 in lymphatic endothelial cells (Cobaleda et al., 2007; Johnson et al., 2008). In CNS, transcription factors identified for their key roles in early neuron development often continue to be expressed in the adult brain and may therefore guard against loss of phenotype or drift into alternative states (Smidt et al., 1997, 2000; Zetterström et al., 1997; Hendricks et al., 1999; Vult von Steyern et al., 1999; Albéri et al., 2004; Simon et al., 2004; Kang et al., 2007; Kittappa et al., 2007; Smidt and Burbach, 2007; Alavian et al.,

2008). However, remarkably little is known of how these factors function at late stages of development or in the adult. Although examples of adult mDA neuron loss has been reported in mice haploinsufficient for transcription factor genes such as *Engrailed* and *FoxA2*, it remains possible that defects originate during embryonic development (Albéri et al., 2004; Zhao et al., 2006; Kittappa et al., 2007; Sonnier et al., 2007). Importantly, FoxA2 and Engrailed are critical for the establishment of the floor plate and for early midbrain/hindbrain development, respectively, and they are directly and indirectly affecting many cell fates along the entire neuraxis. Thus, haploinsufficiency may cause embryonal deficiencies that do not become manifest until adult stages, a possibility that emphasizes the importance of temporally controlled conditional gene targeting to rigorously test how transcription factors function in terminally differentiated neurons.

We do not yet understand why Nurr1 is required in already differentiated mDA neurons. However, data presented here provide compelling evidence for the existence of "terminal selector genes" in mammalian CNS development. Such genes, defined from studies of *Caenorhabditis elegans* neuronal development, are continuously expressed throughout the life of neurons and are essential for both the establishment and maintenance of distinct neuronal phenotypes (Hobert, 2008). Thus, Nurr1, which probably regulates typical mDA neuron markers such as *TH*, *DAT*, *AADC*, and *VMAT2* (Sakurada et al., 1999; Sacchetti et al., 2001; Hermanson et al., 2003; Kim et al., 2003), is likely required for both early differentiation and maintenance by regulating genes that distinguish mDA neurons from other neuron types. Presumably, such regulation is critical throughout the life of mDA neurons and would depend on additional components, such as Pitx3, in a core transcription factor network (Jacobs et al., 2009).

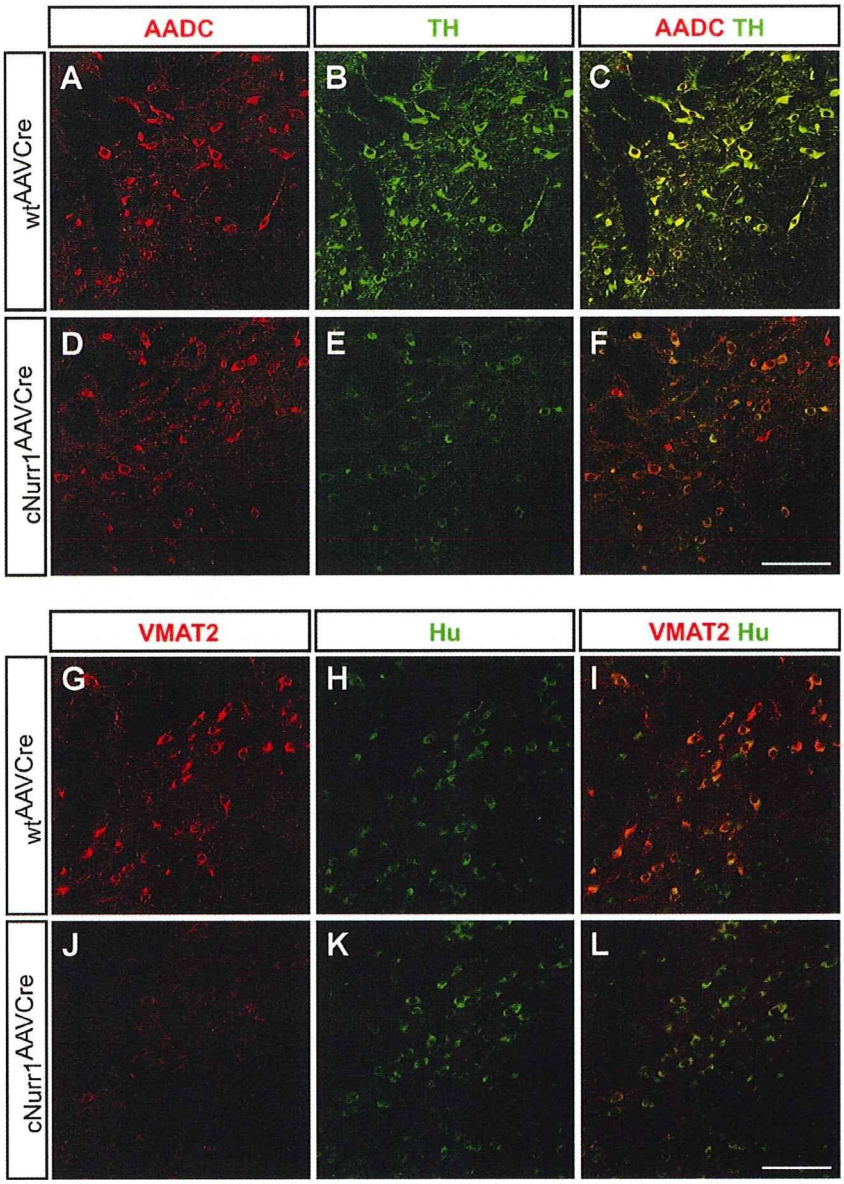

Figure 7. Decreased levels of VMAT2 but not AADC in *cNurr1*^{AAVCre} mice. Confocal analysis of SNc in *wt*^{AAVCre} and *cNurr1*^{AAVCre} mice at 4 months, as indicated. ***A–F***, Confocal images show staining of AADC (red; ***A***, ***D***), TH (green; ***B***, ***E***), and double staining of both markers (***C***, ***F***). Micrographs show that AADC expression appears expressed at normal levels in most cells with decreased levels of TH. ***G–L***, Confocal images show staining for VMAT2 (red; ***G***, ***J***), Hu (***H***, ***K***), and double staining of both markers (***I***, ***L***). Micrographs show that VMAT2 is severely decreased in *cNurr1*^{AAVCre} mice, whereas Hu is maintained at normal levels in essentially all cells with decreased VMAT2. Scale bar, 200 μm.

How may dysregulated Nurr1 activity contribute to PD? Studies in PD patients have shown that, in early stages of the disease, SNc cell bodies are relatively spared compared with the loss of DA in the putamen (Fearnley and Lees, 1991) and that a significant fraction of the surviving, pigmented, DA somata in the SNc have much reduced expression of the TH enzyme (Hirsch et al., 1988; Chu et al., 2006). This suggests that, during early stages of disease, nigral DA neurons may survive in a dysfunctional state characterized by a downregulated neurotransmitter machinery. An interesting possibility supported by our data is that reduced expression of Nurr1 contributes to such symptoms. Indeed, Nurr1 is severely reduced in neurons with signs of pathology in PD brain tissue, and reduced Nurr1 expression in patients' peripheral blood lymphocytes indicates that diminished Nurr1 activity may be a systemic feature of disease (Chu et al., 2006; Le et al., 2008). Although such correlations do not determine whether reduced Nurr1 expression is a cause or a consequence of disease, progressive cell dysfunction in *Nurr1*-ablated mice provides a clear indication that diminished Nurr1 expression in PD should have deleterious consequences for patients. This view is supported by the identification of *Nurr1* gene variants that have been associated with rare cases of familial and sporadic PD (Xu et al., 2002; Le et al., 2003; Zheng et al., 2003; Jankovic et al., 2005; Grimes et al., 2006; Jacobsen et al., 2008). Although other studies have failed to identify such mutations and indicated that Nurr1

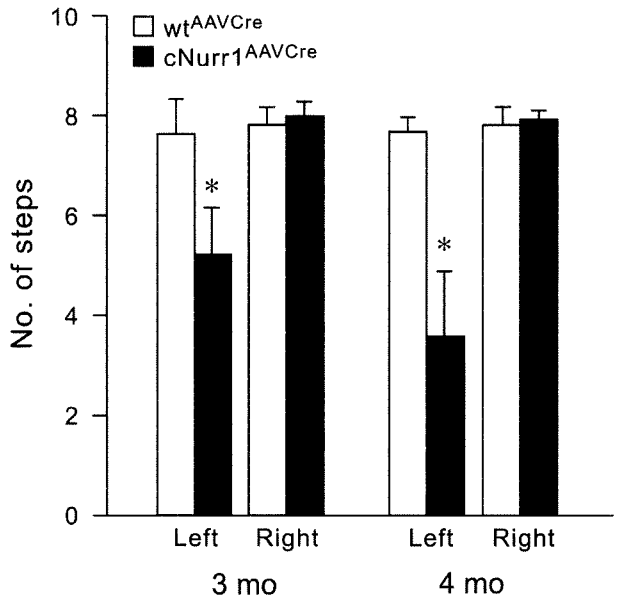

Figure 8. Forelimb akinesia in the stepping test. The performance of the left paw (contralateral to the vector injection) was significantly impaired in the fl/fl mice ($n = 16$) but not the wild-type mice ($n = 13$). Although the impairment was significant at both time points, 3 and 4 months after vector injection, their performance got significantly worse over time ($p < 0.01$, Student's paired t test): 15 of the 16 mice in the fl/fl group showed a decline in their stepping scores between the two tests, and at 4 months, 14 of the fl/fl mice had scores below 5 compared with 6 in the 3 month test. Scores give the means of steps recorded in the forehand and backhand direction for each paw (see Materials and Methods). *$p < 0.001$, Student's paired t test.

gene variants as a cause of PD must be very rare, the combined data from genetics, postmortem PD brain tissue analyses, and the ablation experiments reported here strongly imply that, if and when Nurr1 function is reduced, it will exaggerate PD progression and severity (Wellenbrock et al., 2003; Hering et al., 2004; Tan et al., 2004).

The results indicate that therapies that can restore Nurr1 activity in diseased but not yet degenerated mDA neurons could be of clinical relevance. We envision several strategies whereby Nurr1 activity could be increased. (1) Nurr1 belongs to the nuclear receptor family whose members are commonly regulated by small lipophilic ligands. The putative ligand binding domain of Nurr1 is unconventional and lacks a ligand-binding pocket, but Nurr1 forms heterodimers with retinoid X receptors (RXRs), and ligands activating these receptors can protect mDA neurons in culture (Wallen-Mackenzie et al., 2003; Wang et al., 2003). Thus, RXR may be a relevant target for ligand modulation of Nurr1-regulated processes. It will be important to investigate to what extent Nurr1–RXR heterodimers versus Nurr1 alone are important in pathways associated with the phenotype described in this paper. (2) Nurr1 activity is possible to modulate, for example, by the leukemia drug 6-mercaptopurine (Ordentlich et al., 2003). Although such drugs are pleiotropic and serious side effects are likely, other compounds with higher specificity may be possible to identify. (3) Therapies directed at increasing Nurr1 activity would be effective only as long as sufficient levels of Nurr1 are expressed in diseased neurons. Thus, treatments aimed at restoration of Nurr1 expression by gene delivery may prove advantageous. Using similar AAV vectors as administered in this study may be of particular interest because they have properties that are clinically favorable and are already used in clinical trials in PD patients (Check, 2007).

In conclusion, loss of Nurr1 at stages when characteristic features of mDA neurons are already apparent in the developing embryo or in fully differentiated adult neurons results in loss of mDA neuron-specific gene expression and neuron degeneration. These findings highlight the importance of developmental mechanisms also in the adult brain and clearly indicate that they may be critical for the understanding of cell maintenance and neurodegeneration. How Nurr1 and other transcription factors operate in adult neurons to control and prevent loss or drift in phenotype remains a challenge for future studies.

References

Alavian KN, Scholz C, Simon HH (2008) Transcriptional regulation of mesencephalic dopaminergic neurons: the full circle of life and death. Mov Disord 23:319–328.

Albéri L, Sgadò P, Simon HH (2004) Engrailed genes are cell-autonomously required to prevent apoptosis in mesencephalic dopaminergic neurons. Development 131:3229–3236.

Andersson E, Tryggvason U, Deng Q, Friling S, Alekseenko Z, Robert B, Perlmann T, Ericson J (2006) Identification of intrinsic determinants of midbrain dopamine neurons. Cell 124:393–405.

Breese GR, Knapp DJ, Criswell HE, Moy SS, Papadeas ST, Blake BL (2005) The neonate-6-hydroxydopamine-lesioned rat: a model for clinical neuroscience and neurobiological principles. Brain Res Brain Res Rev 48:57–73.

Castillo SO, Baffi JS, Palkovits M, Goldstein DS, Kopin IJ, Witta J, Magnuson MA, Nikodem VM (1998) Dopamine biosynthesis is selectively abolished in substantia nigra ventral tegmental area but not in hypothalamic neurons in mice with targeted disruption of the Nurr1 gene. Mol Cell Neurosci 11:36–46.

Check E (2007) Second chance. Nat Med 13:770–771.

Chu Y, Le W, Kompoliti K, Jankovic J, Mufson EJ, Kordower JH (2006) Nurr1 in Parkinson's disease and related disorders. J Comp Neurol 494:495–514.

Cobaleda C, Jochum W, Busslinger M (2007) Conversion of mature B cells into T cells by dedifferentiation to uncommitted progenitors. Nature 449:473–477.

Ekstrand MI, Terzioglu M, Galter D, Zhu S, Hofstetter C, Lindqvist E, Thams S, Bergstrand A, Hansson FS, Trifunovic A, Hoffer B, Cullheim S, Mohammed AH, Olson L, Larsson NG (2007) Progressive parkinsonism in mice with respiratory-chain-deficient dopamine neurons. Proc Natl Acad Sci U S A 104:1325–1330.

Fearnley JM, Lees AJ (1991) Ageing and Parkinson's disease: substantia nigra regional selectivity. Brain 114:2283–2301.

Grimes DA, Han F, Panisset M, Racacho L, Xiao F, Zou R, Westaff K, Bulman DE (2006) Translated mutation in the Nurr1 gene as a cause for Parkinson's disease. Mov Disord 21:906–909.

Gurdon JB, Melton DA (2008) Nuclear reprogramming in cells. Science 322:1811–1815.

Hendricks T, Francis N, Fyodorov D, Deneris ES (1999) The ETS domain factor Pet-1 is an early and precise marker of central serotonin neurons and interacts with a conserved element in serotonergic genes. J Neurosci 19:10348–10356.

Hering R, Petrovic S, Mietz EM, Holzmann C, Berg D, Bauer P, Woitalla D, Müller T, Berger K, Krüger R, Riess O (2004) Extended mutation analysis and association studies of Nurr1 (NR4A2) in Parkinson disease. Neurology 62:1231–1232.

Hermanson E, Joseph B, Castro D, Lindqvist E, Aarnisalo P, Wallén A, Benoit G, Hengerer B, Olson L, Perlmann T (2003) Nurr1 regulates dopamine synthesis and storage in MN9D dopamine cells. Exp Cell Res 288:324–334.

Hirsch E, Graybiel AM, Agid YA (1988) Melanized dopaminergic neurons are differentially susceptible to degeneration in Parkinson's disease. Nature 334:345–348.

Hobert O (2008) Regulatory logic of neuronal diversity: terminal selector genes and selector motifs. Proc Natl Acad Sci U S A 105:20067–20071.

Huot P, Parent A (2007) Dopaminergic neurons intrinsic to the striatum. J Neurochem 101:1441–1447.

Jacobs FM, van Erp S, van der Linden AJ, von Oerthel L, Burbach JP, Smidt MP (2009) Pitx3 potentiates Nurr1 in dopamine neuron terminal dif-

ferentiation through release of SMRT-mediated repression. Development 136:531–540.

Jacobsen KX, MacDonald H, Lemonde S, Daigle M, Grimes DA, Bulman DE, Albert PR (2008) A Nurr1 point mutant, implicated in Parkinson's disease, uncouples ERK1/2-dependent regulation of tyrosine hydroxylase transcription. Neurobiol Dis 29:117–122.

Jain S, Golden JP, Wozniak D, Pehek E, Johnson EM Jr, Milbrandt J (2006) RET is dispensable for maintenance of midbrain dopaminergic neurons in adult mice. J Neurosci 26:11230–11238.

Jankovic J, Chen S, Le WD (2005) The role of Nurr1 in the development of dopaminergic neurons and Parkinson's disease. Prog Neurobiol 77:128–138.

Johnson NC, Dillard ME, Baluk P, McDonald DM, Harvey NL, Frase SL, Oliver G (2008) Lymphatic endothelial cell identity is reversible and its maintenance requires Prox1 activity. Genes Dev 22:3282–3291.

Kang BJ, Chang DA, Mackay DD, West GH, Moreira TS, Takakura AC, Gwilt JM, Guyenet PG, Stornetta RL (2007) Central nervous system distribution of the transcription factor Phox2b in the adult rat. J Comp Neurol 503:627–641.

Kim KS, Kim CH, Hwang DY, Seo H, Chung S, Hong SJ, Lim JK, Anderson T, Isacson O (2003) Orphan nuclear receptor Nurr1 directly transactivates the promoter activity of the tyrosine hydroxylase gene in a cell-specific manner. J Neurochem 85:622–634.

Kirik D, Rosenblad C, Björklund A (1998) Characterization of behavioral and neurodegenerative changes following partial lesions of the nigrostriatal dopamine system induced by intrastriatal 6-hydroxydopamine in the rat. Exp Neurol 152:259–277.

Kittappa R, Chang WW, Awatramani RB, McKay RD (2007) The foxa2 gene controls the birth and spontaneous degeneration of dopamine neurons in old age. PLoS Biol 5:e325.

Kramer ER, Aron L, Ramakers GM, Seitz S, Zhuang X, Beyer K, Smidt MP, Klein R (2007) Absence of Ret signaling in mice causes progressive and late degeneration of the nigrostriatal system. PLoS Biol 5:e39.

Le W, Pan T, Huang M, Xu P, Xie W, Zhu W, Zhang X, Deng H, Jankovic J (2008) Decreased NURR1 gene expression in patients with Parkinson's disease. J Neurol Sci 273:29–33.

Le WD, Xu P, Jankovic J, Jiang H, Appel SH, Smith RG, Vassilatis DK (2003) Mutations in NR4A2 associated with familial Parkinson disease. Nat Genet 33:85–89.

Oo TF, Kholodilov N, Burke RE (2003) Regulation of natural cell death in dopaminergic neurons of the substantia nigra by striatal glial cell line-derived neurotrophic factor *in vivo*. J Neurosci 23:5141–5148.

Ordentlich P, Yan Y, Zhou S, Heyman RA (2003) Identification of the antineoplastic agent 6-mercaptopurine as an activator of the orphan nuclear hormone receptor Nurr1. J Biol Chem 278:24791–24799.

Pascual A, Hidalgo-Figueroa M, Piruat JI, Pintado CO, Gómez-Díaz R, López-Barneo J (2008) Absolute requirement of GDNF for adult catecholaminergic neuron survival. Nat Neurosci 11:755–761.

Perlmann T, Wallén-Mackenzie A (2004) Nurr1, an orphan nuclear receptor with essential functions in developing dopamine cells. Cell Tissue Res 318:45–52.

Sacchetti P, Brownschidle LA, Granneman JG, Bannon MJ (1999) Characterization of the 5′-flanking region of the human dopamine transporter gene. Brain Res Mol Brain Res 74:167–174.

Sacchetti P, Mitchell TR, Granneman JG, Bannon MJ (2001) Nurr1 enhances transcription of the human dopamine transporter gene through a novel mechanism. J Neurochem 76:1565–1572.

Sakurada K, Ohshima-Sakurada M, Palmer TD, Gage FH (1999) Nurr1, an orphan nuclear receptor, is a transcriptional activator of endogenous tyrosine hydroxylase in neural progenitor cells derived from the adult brain. Development 126:4017–4026.

Saucedo-Cardenas O, Quintana-Hau JD, Le WD, Smidt MP, Cox JJ, De Mayo F, Burbach JP, Conneely OM (1998) Nurr1 is essential for the induction of the dopaminergic phenotype and the survival of ventral mesencephalic late dopaminergic precursor neurons. Proc Natl Acad Sci U S A 95:4013–4018.

Schallert T, Norton D, Jones TA (1992) A clinically relevant unilateral rat model of Parkinsonian akinesia. J Neural Transpl Plast 3:332–333.

Simon HH, Thuret S, Alberi L (2004) Midbrain dopaminergic neurons: control of their cell fate by the engrailed transcription factors. Cell Tissue Res 318:53–61.

Smidt MP, Burbach JP (2007) How to make a mesodiencephalic dopaminergic neuron. Nat Rev Neurosci 8:21–32.

Smidt MP, van Schaick HS, Lanctôt C, Tremblay JJ, Cox JJ, van der Kleij AA, Wolterink G, Drouin J, Burbach JP (1997) A homeodomain gene Ptx3 has highly restricted brain expression in mesencephalic dopaminergic neurons. Proc Natl Acad Sci U S A 94:13305–13310.

Smidt MP, Asbreuk CH, Cox JJ, Chen H, Johnson RL, Burbach JP (2000) A second independent pathway for development of mesencephalic dopaminergic neurons requires Lmx1b. Nat Neurosci 3:337–341.

Smidt MP, Smits SM, Burbach JP (2004) Homeobox gene Pitx3 and its role in the development of dopamine neurons of the substantia nigra. Cell Tissue Res 318:35–43.

Snyder AM, Zigmond MJ, Lund RD (1986) Sprouting of serotoninergic afferents into striatum after dopamine-depleting lesions in infant rats: a retrograde transport and immunocytochemical study. J Comp Neurol 245:274–281.

Sonnier L, Le Pen G, Hartmann A, Bizot JC, Trovero F, Krebs MO, Prochiantz A (2007) Progressive loss of dopaminergic neurons in the ventral midbrain of adult mice heterozygote for Engrailed 1. J Neurosci 27:1063–1071.

Soriano P (1999) Generalized lacZ expression with the ROSA26 Cre reporter strain. Nat Genet 21:70–71.

Takahashi K, Yamanaka S (2006) Induction of pluripotent stem cells from mouse embryonic and adult fibroblast cultures by defined factors. Cell 126:663–676.

Tan EK, Chung H, Chandran VR, Tan C, Shen H, Yew K, Pavanni R, Puvan KA, Wong MC, Teoh ML, Yih Y, Zhao Y (2004) Nurr1 mutational screen in Parkinson's disease. Mov Disord 19:1503–1505.

Vult von Steyern F, Martinov V, Rabben I, Njå A, de Lapeyrière O, Lømo T (1999) The homeodomain transcription factors Islet 1 and HB9 are expressed in adult alpha and gamma motoneurons identified by selective retrograde tracing. Eur J Neurosci 11:2093–2102.

Wallen-Mackenzie A, Mata de Urquiza A, Petersson S, Rodriguez FJ, Friling S, Wagner J, Ordentlich P, Lengqvist J, Heyman RA, Arenas E, Perlmann T (2003) Nurr1-RXR heterodimers mediate RXR ligand-induced signaling in neuronal cells. Genes Dev 17:3036–3047.

Wang Z, Benoit G, Liu J, Prasad S, Aarnisalo P, Liu X, Xu H, Walker NP, Perlmann T (2003) Structure and function of Nurr1 identifies a class of ligand-independent nuclear receptors. Nature 423:555–560.

Wellenbrock C, Hedrich K, Schafer N, Kasten M, Jacobs H, Schwinger E, Hagenah J, Pramstaller PP, Vieregge P, Klein C (2003) NR4A2 mutations are rare among European patients with familial Parkinson's disease. Ann Neurol 54:415.

Xu PY, Liang R, Jankovic J, Hunter C, Zeng YX, Ashizawa T, Lai D, Le WD (2002) Association of homozygous 7048G7049 variant in the intron six of Nurr1 gene with Parkinson's disease. Neurology 58:881–884.

Zetterström RH, Williams R, Perlmann T, Olson L (1996) Cellular expression of the immediate early transcription factors Nurr1 and NGFI-B suggests a gene regulatory role in several brain regions including the nigrostriatal dopamine system. Brain Res Mol Brain Res 41:111–120.

Zetterström RH, Solomin L, Jansson L, Hoffer BJ, Olson L, Perlmann T (1997) Dopamine neuron agenesis in Nurr1-deficient mice. Science 276:248–250.

Zhao ZQ, Scott M, Chiechio S, Wang JS, Renner KJ, Gereau RW 4th, Johnson RL, Deneris ES, Chen ZF (2006) Lmx1b is required for maintenance of central serotonergic neurons and mice lacking central serotonergic system exhibit normal locomotor activity. J Neurosci 26:12781–12788.

Zheng K, Heydari B, Simon DK (2003) A common NURR1 polymorphism associated with Parkinson disease and diffuse Lewy body disease. Arch Neurol 60:722–725.

分光測定入門シリーズ 8

日本分光学会 [編]
The Spectroscopical Society of Japan

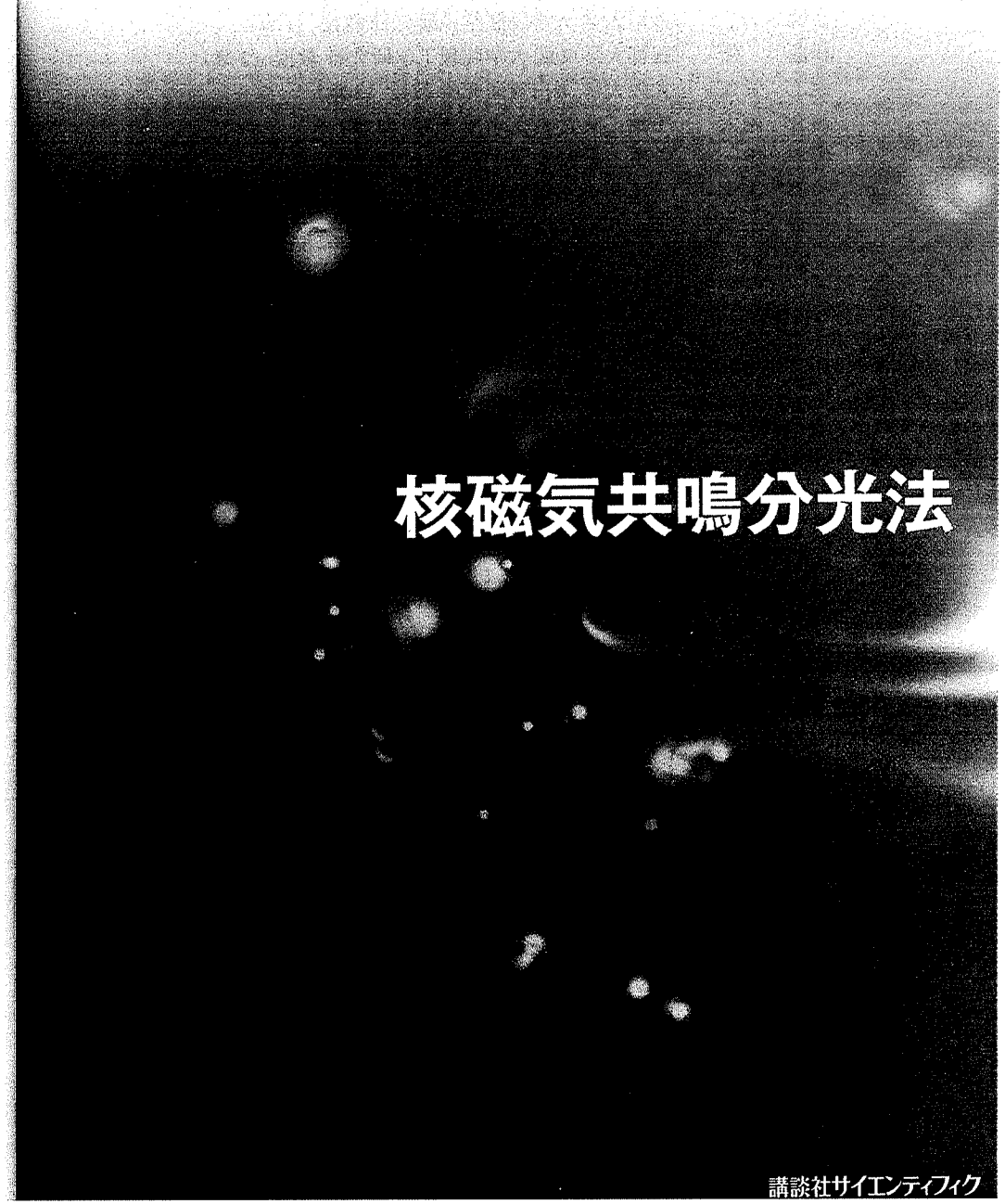

核磁気共鳴分光法

講談社サイエンティフィク

1
NMR の原理

1.1 はじめに— NMR 発展の歴史とノーベル賞—

いくつかの原子核は強い磁場中に置かれると，特定のエネルギーの電磁波を吸収するような性質をもつようになる．核磁気共鳴法（nuclear magnetic resonance，NMR）はこの性質を利用した分光法である[1,2]．近年，分光分析法における NMR の重要性は，ますます増加しつつあるが，にもかかわらず初心者（特に化学系や生物系の学生で物理や数学が苦手な人たち）が学ぶには敷居が高いことは否めない．一つには NMR の発見の歴史から見て明らかなように，1940 ～ 1950 年代にかけて，核スピンや電子スピンと NMR 現象が発見された当初，NMR の話題の中心が物理学と量子力学であっ

表 1.1 ノーベル賞から見た NMR 発展の歴史

	受賞理由	受賞者	受賞したノーベル賞
物理の時代	核スピン・電子スピンの発見	W. Pauli	ノーベル物理学賞 (1945)
		P. Kusch	ノーベル物理学賞 (1955)
	NMR 現象の発見	I. I. Rabi	ノーベル物理学賞 (1944)
		E. M. Purcell	ノーベル物理学賞 (1952)
		F. Bloch	ノーベル物理学賞 (1952)
	超伝導現象の発見	H. K. Onnes	ノーベル物理学賞 (1913)
		J. Bardeen ら	ノーベル物理学賞 (1972)
化学の時代	二次元 NMR	R. R. Ernst	ノーベル化学賞 (1991)
医学・生物学の時代	タンパク質の NMR による立体構造決定	K. Wüthrich	ノーベル化学賞 (2002)
	MRI による画像解析法	P. Mansfield	ノーベル生理学・医学賞 (2003)
		P. Lauterbur	ノーベル生理学・医学賞 (2003)

たためであろう．その後，半世紀以上にわたる技術革新と装置の高度化が続けられてきた結果，高分解能 NMR 技術は 20 世紀後半に爆発的に発展した．こうした，NMR が「化学の時代」を経て「医学・生物学の時代」へと遷移しながら発展を続けているという経緯は，NMR 現象に関連のある成果に対して授与されたノーベル賞のリストからも見て取れる（表 1.1）．2002 年の K. Wüthrich 博士，2003 年の P. Mannsfield 博士，P. Lauterber 博士らの NMR に関連する応用研究が二年連続してノーベル賞に輝いたことは記憶に新しい．

現在，NMR は溶液中の分子構造決定をはじめとして，固体物性研究のための固体 NMR や，生体分子を解析する構造生物学，代謝産物の混合物を網羅的に解析するメタボロミクス，画像診断を通じた医療への応用へと幅広い広がりを見せており，分光法の中でも特別な地位を占めている．その一方で，NMR 現象は，強い磁場中に置かれた原子核と電磁波の相互作用を利用した分光法であり，核スピンの量子力学的なふるまいについて，理論と実験がきわめてよく一致する方法論である．たとえば，測定中に各核スピンにおける量子力学的重ね合わせ状態を人工的に実現でき，しかもそれを任意に操作することができるので量子コンピューティングの装置としても注目されている．しかし，限られたスペースで，初学者の理解を優先するために，難しい量子力学や数学の話は他の成書[3～5]に譲ることとして，本書では NMR を使ううえでの最低限の注意事項などを中心に説明することにする．実際，筆者の実感としては，後述する分極移動の項以外は，量子力学をほとんど知らなくても（古典的なモデルのみで）NMR 現象の概要が理解できる．

1.2 NMR の原理

1.2.1 核スピンとは

NMR とは核スピンの状態を観測する計測手法である．核スピンとは，原子や電子の状態を記述する波動方程式に出てくる量子数のうち，主量子数 n，方位量子数 l，磁気量子数 m の後に見出された第四の量子数（スピン量子数 s）に由来する物理量のことであり，記号 I で表す．スピンを古典力学的にイメージしようとするならば，荷電粒子がそれ自体で「自転」するときに生じる磁気モーメントに対応し，原子核だけでなく電子にも存在する．電子のスピンは 1/2 であり，外部の静磁場により +1/2 と −1/2 の 2 つのエネルギー準位に分裂する（Zeeman 分裂）．2 つのエネルギー差に相当する周波数の電磁波を照射されると，電子スピンは共鳴して，安定状態から励起状態

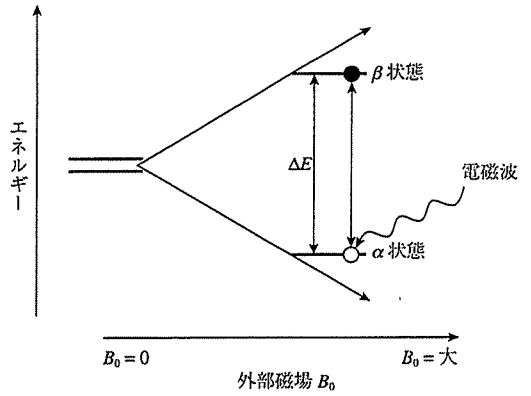

図 1.1 Zeeman 分裂
外部磁場により縮重していた核スピンの 2 つのエネルギー状態が分裂し，エネルギー差に相当する電磁波を吸収するようになる．

に遷移する（図 1.1）．この原理を利用した測定法が電子スピン共鳴法（electron spin resonance，ESR）であり，遷移金属化合物やラジカル分子の電子的性質を調べるのに用いられている．同様に，核スピンは 1/2，1，3/2，2，…のように半整数または整数のとびとびの値をもち，エネルギー準位の分裂が起き，エネルギー差に相当する電磁波を吸収して核のスピン状態が変化する．これが核磁気共鳴法（NMR）である．装置開発の歴史的な経緯から，ESR では照射する電磁波の周波数を固定して外部の磁場の強さを変えていくのに対し，NMR では磁場の強さを一定にしておいて，周波数を変化させる方法が採られ，その後，一度吸収された電磁波が再放出される過程を計測するパルスフーリエ変換（Fourier transform，FT）－NMR へと変化した（後述）．

1.2.2 NMR で観測可能な核種

さて，原子はそれぞれの原子核の原子番号と質量数に応じて，固有の核スピン値をもっている．一般的には，質量数が奇数の原子は 1/2，3/2，5/2 などの半整数の値を，質量数が偶数かつ原子番号が奇数の原子は 1，2，3 などの整数の値をとる．質量数が偶数かつ原子番号が偶数の原子ではスピンは 0 となる．NMR 現象は，この核スピンが 0 でないすべての原子において可能である．しかし，$I \geqq 1$ の核では NMR の吸収線の線幅の広幅化が起こるため高分解能 NMR に適さない．一方，特に $I = 1/2$ の核種では線幅の鋭い信号が得られるため，理論的取り扱いが容易なことも相まって，よく利用されるようになった．化学・生物学分野でよく利用される原子核の例を表 1.2 に